We are IntechOpen, the world's leading publisher of Open Access books Built by scientists, for scientists

4,800
Open access books available

122,000
International authors and editors

135M
Downloads

Our authors are among the

154
Countries delivered to

TOP 1%
most cited scientists

12.2%
Contributors from top 500 universities

CLARIVATE ANALYTICS BOOK CITATION INDEX INDEXED

WEB OF SCIENCE™

Selection of our books indexed in the Book Citation Index in Web of Science™ Core Collection (BKCI)

Interested in publishing with us?
Contact book.department@intechopen.com

Numbers displayed above are based on latest data collected.
For more information visit www.intechopen.com

8

Analysis and Mitigation of Icing Effects on Wind Turbines

Adrian Ilinca
Wind Energy Research Laboratory, Université du Québec à Rimouski
Canada

1. Introduction

Precipitation, atmospheric and in-cloud icing affect wind turbine operation in various ways, including measurement and control errors, power losses, mechanical and electrical failures and safety hazard. Anti-icing and de-icing strategies are used to minimize these effects. Many active and passive methods are in development but few are available on the market. Active heating of blades is the most tested, used and reliable way to prevent icing effects. It is used in parallel with passive hydrophobic coating to lower energy consumption. Precise icing evaluation of the site should be done during the assessment phase to evaluate the necessity and benefits of installing anti-icing and/or de-icing system. This evaluation shall continue during operation in order to optimize production and avoid component failure related to icing events. Multiple anemometry in combination with relative humidity measurements is a cheap and reliable icing detection method during assessment while the use of ice sensors and the power curve method is recommended during operation. Most of the wind turbines operating in cold climates are facing icing events, but very few of them are equipped with blade de-icing systems, and few studies were performed and published on the characteristics of these systems.

Technical difficulties due to cold climate conditions have occurred for most of the existing projects in Quebec. Thus, icing simulations were carried out in the refrigerated wind tunnel of the Anti-icing Materials International Laboratory (AMIL) at Université du Québec à Chicoutimi (UQAC). The effect of icing conditions observed at the wind farm in Murdochville, Québec, Canada has been assessed on a 0.2 m NACA63-415 blade airfoil. The shape and mass of the ice deposit on a wind turbine airfoil has been measured, as well as the lift and drag force on the iced airfoil. Scaling was carried out based on the 1.8 MW–Vestas V80 wind turbine technical data, for three different radial positions and two in-fog icing conditions measured at the Murdochville wind farm in the Gaspé Peninsula. For both icing events, the mass of ice accumulated on the blade airfoil increased as we move to the tip of the blade. In wet regime, glaze formed mostly near the leading edge and on the pressure side. It also accumulated by run-off on the trailing edge of the outer half of the blade. In dry-regime, rime mostly accreted on the leading edge and formed horns. For both icing events, when glaze or rime accreted on the blade airfoil, lift decreased and drag increased. A load calculation using the blade element theory shows that drag force on the entire blade becomes too large compared to lift, leading to a negative torque and the stop of the wind turbine. Torque reduction is more significant on the outer third of the blade. Setting up a de-

icing system only on the outer part of the blade would enable significant decrease of heating energy costs. In order to optimize the design and power consumption of an electro-thermal de-icing system for wind turbine blades, an experimental setup was built and used to test the system under similar icing conditions. The parameters of the de-icing control system consider only the convective heat loss at the blade surface during ice accretion. The results show the relation among the meteorological conditions, the ridge formed by liquid water runback, the heating power and the airfoil surface temperature. The study provides useful data for the design of electro-thermal de-icing systems for wind turbine blade application.

2. Ice accretion effects on wind turbines

Wind turbines (WT) operating in cold regions or at high altitudes are frequently facing icing conditions during winter operation. At the same time, the best sites for wind farm installation are located at higher altitudes, as wind speed generally increases by 0.1m/s per 100m of altitude for the first 1000m. In regions with cold climate, available wind power is approximately 10% higher than in other regions due to increased air density at lower temperatures (Fortin et al., 2005a). Therefore, wind farms installed in some of the best wind sites around the world are facing possible icing events. Icing affects the wind assessment and the operation of wind farms. The following problems are directly related to icing and cold climate: measurement errors, power losses, overproduction, mechanical failures, electrical failures and safety hazards.

Measurement errors: during the assessment phase, the anemometers, wind vanes and temperature sensors can be affected by ice. In icing conditions, wind speed errors can be as high as 30% (Laakso et al., 2003a). Another study identifies a maximum error of 40% for an ice-free anemometer and 60% for a standard anemometer during icing events (Fortin et al., 2005b);

Power losses: ice accretion changes the shape and roughness of the blade airfoil (consequently affecting their aerodynamic characteristics) and introduces measurement errors from turbine instruments (wrong wind speed or direction, which affects yaw and power controls). Small amounts of ice on the leading edge of airfoils significantly reduce aerodynamic properties of the blade and the resulting power production (Marjaniemi and Peltola, 1998). Power losses may vary from 0.005 to 50% of the annual production, depending on icing intensity and its duration on the site, wind turbine models and the evaluation methodology (Botta et al., 1998; Gillenwater, 2008; Laakso et al., 2005b; Tammelin et al., 2005);

Overproduction: Higher air density related to low temperatures and airfoil modifications can lead to overproduction of the WT. Overproduction of up to 16% has been recorded (Jasinski et al., 1997);

Mechanical failures: ice accretion will increase the load on the blades and on the tower structure, causing high amplitude vibrations and/or resonance as well as mass imbalance between blades. Operation at low temperatures affects oil viscosity and changes the dimensions and mechanical properties of different components of the WT. This results in possible overheating and higher fatigue charges on components; one of the most affected being gearboxes whose lifetime is considerably reduced (Botta et al., 1998; Laakso and Peltola, 2005; Seifert, 2003; Tammelin et al., 2005);

Electrical failure: snow infiltration in nacelle and extreme temperature lead to condensation in the electronics (Laakso et al., 2003a);

Safety hazard: large icing accumulation on blades can be thrown at a distance of up to 1.5 x the combined height of the turbine and the rotor diameter (Tammelin et al., 2000). Using a Monte-Carlo simulation, Battisti et al. (Battisti et al., 2005b) have shown that the odds to be hit by a piece of ice (between 0.18 and 0.36kg), on a site with moderate icing conditions (5 days per year), is 1 in 10. This is valid for a person walking 10 hours under an operating turbine that uses a de-icing system, considering a total ice accretion of 75kg/rotor per day.

2.1 Physics of atmospheric icing

There are three types of atmospheric icing related to wind turbine: in-cloud, precipitation and frost (Boluk, 1996; Fikke et al., 2006; ISO-12494, 2001; Richert, 1996).

In-cloud icing: it happens when super-cooled water droplets hit a surface below 0°C and freeze upon impact. The droplets temperature can be as low as -30°C and they do not freeze in the air, because of their size. Accretions have different sizes, shapes and properties, depending on the number of droplets in the air (liquid water content - *LWC*) and their size (median volume diameter - *MVD*), the temperature, the wind speed, the duration, the chord length of the blade and the collection efficiency. There is a continuum of ice accretion appearance from rime at coldest temperatures to glaze at warmest.

Soft rime: thin ice with needles and flakes. Appears when temperature is well below 0°C and the MVD and LWC are small. The resulting accretion will have low density and little adhesion.

Hard rime: higher MVD and LWC will cause accretion with higher density, which is more difficult to remove.

Glaze: when a portion of the droplet does not freeze upon impact, but run back on the surface and freezes later. The resulting ice density and adhesion are strong. It is often associated with precipitation.

Precipitation: can be snow or rain. The accretion rate can be much higher than in-cloud, which causes more damage.

Freezing rain: when rain falls on a surface whose temperature is below 0°C. It often occurs during inversion. Ice density and adhesion are high when this phenomenon occurs.

Wet snow: when snow is slightly liquid at air temperature between 0 and -3°C, it sticks to the surface. It is easy to remove at first, but can be difficult if it freezes on the surface.

Frost: appears when water vapour solidifies directly on a cool surface. It often occurs during low winds. Frost adhesion may be strong.

2.2 Ice accretion measurement

The estimation of ice accretion on solid surfaces can be done using direct measurement, indirect measurement or numerical modelling. Direct methods are based on the detection of some change of physical property caused by ice accretion. These include mass, reflective properties, electrical or thermal conductivity, dielectric coefficient and inductance. Indirect methods are based on detecting weather conditions that lead to icing, such as humidity, temperature and wind speed or detecting the effects of icing, such as a reduction in power production. Then, an empirical or deterministic model is used to determine when icing occurs to evaluate the LWC and MVD, (Homola et al., 2006). Meteorological numerical prediction models have the capability to determine with some accuracy the severity and duration of icing events.

2.3 Icing evaluation during site sssessment

When the financial benefits of a blade heating system are evaluated, parameters like the icing duration and severity, as well as potential wind resources, need to be known (Laakso et al., 2003a). How cost-effective is this operation is depending on the available wind energy during the icing period and on the severity of icing. This analysis requires knowledge of both the meteorological conditions leading to ice accretion and the turbine's geometry and operating conditions. The meteorological parameters needed for ice prevention design are well known and draw on over 50 years of experimental investigation in the aeronautic field. They are mainly the liquid water content (LWC), water droplet diameter (MVD), pressure, temperature, and the horizontal distribution of these variables. One reason for the scarce use of these parameters is that they are difficult or expensive to measure. Quantitative data are hardly ever available for assessing either icing frequency or icing severity at a given site (Battisti et al., 2005a). Measurement of the icing duration is so difficult that, most of the time, it has to be estimated empirically (Kimura et al., 2000). In some conditions, it has been observed that measurements as close as 1km from a specific site may not give reliable information (Laakso et al., 2003a). It is thus recommended to measure icing events directly at the planned implementation site (Fikke et al., 2006). A significant difficulty stems from the fact that ice measurement should be done at the same height as the top blade tip (Homola et al., 2006). This section presents the most frequent methods and models to evaluate icing.

Ice sensors: The ISO-12494 norm proposes an ice mass measurement method using an ice collector that consists of a 30mm diameter cylinder, with a minimum length of 0.5m that slowly rotates around a vertical axis (ISO-12494, 2001). This technique provides poor information indicative of icing risks for wind turbines. In fact, wind velocity and the dimension of the cylinder are far out of the range of relative velocities and leading edge diameters of wind turbine blades (Battisti et al., 2005a). Other sensors, using different approaches, such as longitudinal wire waves, vibrating probes or optics exist, but they are mostly used during the operation phase. The main reason these sensors are not commonly used on remote met masts is because of their high costs and their energy demands. Also, different sensors have been tested thoroughly (Fikke et al., 2005; Tammelin et al., 2005) and none of them has perfect reliability and accuracy. The different ice sensors generated significant differences in the recording of icing events and the different sensors did not always indicate icing synchronously (Tammelin et al., 2005). Ice sensors also underestimate icing because of the heating cycle (Laakso et al., 2003b). It has been proposed to improve the predictions by using two detectors, one heated for intensity and one unheated for duration (Tammelin et al., 2005).

Double anemometry and vane: An icing event is assumed when the difference between the wind speeds measured by heated and unheated anemometers exceeds a certain limit. Tallhaug suggests a limit of 20% at wind speeds above 2 m/s (Tallhaug, 2003). Laakso (Laakso et al., 2003b) considers that a value of ± 5% is more appropriate. A larger difference, e.g. ± 10%, would have resulted in only few data sets to indicate icing, which represents too little icing time compared to the ice amounts that can be seen on photos. Craig suggests a method that uses three anemometers: one permanently heated, one unheated and one heated when a 15% difference is observed between the speeds of the heated and unheated anemometers (Craig and Craig, 1996). Equipping the measurement mast with one properly heated and one unheated anemometer to estimate wind resource measurements is cheap and advisable. This arrangement gives an overall picture of ice climate. These methods, in

addition to relative humidity measurements, may give a fairly good idea of the time that ice is likely to affect wind turbines operation (Laakso et al., 2005).

Tallhaug (Tallhaug, 2003) proposes to use an unheated wind vane and assumes that an icing event occurs when the unheated wind vane has zero standard deviation calculated from 6 following 10- minute averages and at temperatures below zero. He showed that there is a very good correlation between zero standard deviation on the unheated direction sensor and the double anemometry indication.

A disadvantage of the double anemometry method lies in the fact that the anemometers are lower than the tip of the blades, where there is more icing (Tammelin et al., 2005). Also, the method works well at relatively mild temperatures (around 0°C). Otherwise, the unheated anemometer may stay frozen for longer periods (Craig and Craig, 1996). On the other hand, the double anemometry can measure the persistency of icing (Laakso et al., 2003b). Results showed that it is possible to estimate the total period during which an icing event will affect the operation of the WT (comments from (Laakso et al., 2003b) on (Craig and Craig, 1996)), by studying its correlation with the period during which ice affects the unheated anemometer. This duration is obviously longer than the actual icing period.

Another disadvantage is that low temperatures were found to cause negative errors for unheated anemometers (i.e. the difference between heated and unheated anemometers did not result from icing (Laakso et al., 2003b)). It is difficult to determine when icing occurs only from wind speed measurement as the unheated anemometer shows both higher and lower wind speeds. Higher values of unheated anemometers have also been observed during snowfall (Seifert, 2003). Obviously, double anemometry will give no indication of icing at zero wind. At very low wind speed, the difference between heated and unheated anemometers can be explained by their different inertial characteristics rather than actual icing.

Relative humidity and dew point: Because relative humidity is high during in-cloud icing, the detection of high humidity (>95%) combined with low temperature (<0°C) is used to detect icing. A dew point detector that has been designed for subzero operation could provide valuable information, because in practice air temperature is at frost point nearly all the time when in-cloud icing occurs (Laakso et al., 2005b). Measuring the relative humidity with temperature is used much more often than the dew point measurement. However, this method has not detected icing events during the same period as ice detectors (Tammelin et al., 2005). It has been shown that 33% of all ice detector indications at 84m level occurred when relative humidity was lower than 95% (Laakso et al., 2003b). The predictability of icing events using conditions of relative humidity of more than 95-98% with temperature less than 0°C is weak. On many occasions, the temperature was below 0°C with relative humidity higher than 95% and no icing was observed (Tammelin et al., 2005).

Visibility and cloud base: In-cloud icing occurs when a structure is surrounded by a cloud at a temperature below 0°C with a minimal wind speed of around 2m/s. The cloud can be detected using the cloud base height or the horizontal visibility. Clouds are classified using qualitative quotes or visibility distance to estimate the liquid water content (LWC), which directly affects the intensity of the in-cloud icing. This is done using airport observation, a pyranometer, video monitoring or automatic sensors. Airport observation provides cloud base heights and a cloudiness index based on the observation of the cloud density, on a scale from 1 to 8. When the index is higher than 6/8 and the cloud base height is lower than the wind turbine, icing is detected or the index can be used as a ratio for accretion intensity (Tallhaug, 2003). The pyranometer measures the solar radiation intensity. It has been observed that when the intensity is lower than 300W/m², ice is detected (Kimura et al.,

2000). Video monitoring can measure horizontal visibility using painted poles at distances from 50 m up to 300m from met mast (Dobesch et al., 2003). The use of painted poles gives a numerical criterion of the cloud density (Tammelin et al., 2005). Finally, automatic detection can be done using radar and microwave radiometers which can directly detect the LWC (Battisti et al., 2005a). Unfortunately, this method is too expensive and not commonly used during site assessment.

Acquiring information, such as time series of cloud base heights from the nearest airport, and comparing them with the measured data is also advisable. This method and double anemometry are likely to give a fairly good idea of the time period that ice is likely to affect the operation of the wind turbines (Laakso et al., 2005b). However, cloud height observed at the nearby weather station does not necessarily represent accurately onsite cloud conditions and it is preferable to measure the horizontal visibility on the specific site to estimate in-cloud icing. Even under these conditions, the method underestimates the real ice mass (Tammelin et al., 2005).

Aeronautics considers that icing events occur for specific values of meteorological variables: wind speed V>0, temperature T<0, liquid water content LWC>0 and median volumetric droplet diameter MVD. When such limits are simultaneously exceeded, ice will form. The direct icing duration (icing time) is defined as the minimum duration of the single event with a contemporary occurrence of LWC>0, T<0 and V>0. The intensity of the phenomenon can only be determined if turbine's geometrical features and operating conditions are given. The most important specific wind turbine parameters are the relative wind velocity, the dimension and surface properties of the airfoils subjected to icing. Correlations between LWC and MVD with base cloud heights (CH) are valid for each specific site condition. On the other hand, the range of altitudes at which icing can occur is condition specific. Thus, extrapolating from aeronautical data produces uncertain results. For mountainous sites, significant influence of topography complicates the issue (Battisti et al., 2005a).

An alternative to this technique is the creation of an ice map. Several papers have been published with the objective of creating an icing map that would directly give the number of icing days with respect to the location. In Europe, this map was introduced by Makkonen and Ahti (Makkonen and Ahti, 1995), using cloud height (CH<200m), wind speed (V>0) and temperature (T<0) as conditions for ice accretion. They also found that the severity of rime ice is strongly related to the terrain roughness. The altitude relative to the sea level (ASL) does not significantly affect the calculated ice loads but the elevation in relation to the local terrain configuration (topography and roughness) does. Later, it has been found that this formula strongly overestimated icing, probably because of wrong wind speed measurement during icing events. A corrected equation was therefore proposed (Tammelin and Säntti, 1996). Later, comments on this equation mentioned that wind speed and temperature should be taken at a 200m height above ground. However, it remains that this formula can only provide a rough estimation of the amount of rime accretion (Tammelin and Säntti, 1998). The use of heated anemometers under similar conditions results in a smaller quantity of ice (Tammelin et al., 2000). Finally, Dobesh adds the visibility factor (Dobesch et al., 2003). He considers that icing occurs when the following conditions are met:

$$\begin{cases} T_{200m} < 0^{o}C \\ CH < 200m \; or \; Visibility < 300m \\ V_{200m} > 0 \end{cases} \quad (1)$$

The introduction of horizontal visibility conditions takes into account that frequently no cloud height is observed during foggy weather conditions. The commonly used value of 1,000m for "visibility" in meteorology is not useful to predict icing. The visibility should be less than 300 meters to observe icing using the LWC. Dobesh concluded that the effect of solar radiation on icing duration does not improve the estimation of icing event maps at the site scale (Dobesch et al., 2003). Indeed, during winter, especially at higher latitudes, the intensity of solar radiation is too weak to enhance significant melting processes at low temperatures. Also, it is very difficult to get accurate data because the radiation network is very sparse and the use of analytical models is quite uncertain for the time span of one to several hours during the day.

Furthermore, wind turbines react differently to icing (Tammelin et al., 2005). A tool for estimating the number of icing days and icing intensity at a given site is still missing. Due to local topography, great variations in icing severity and intensity are observed within short distances. Therefore, icing maps cannot be interpreted as exact and must be used in connection with local topographical information and, if possible, measurement statistics (Laakso et al., 2003a).

Models: Physical mesoscale models (MM5, MC2 and others), generally used in regional weather prediction, can be used to predict upcoming icing events or the likelihood of such events for specific projects or time frames. More sophisticated empirical or statistical models consider additional parameters such as temperature (air, object, wet-bulb and dew point), wind direction, wind speed, cloud height, cloud cover, the humidity profile, precipitation, regional topography, local topography, object size, shape and material composite and solar radiation. These models can now provide information about the amount and rate of icing instead of just the frequency of icing events (Laakso et al., 2003a).

Other methods: Visual detection uses video filming of guy wires during icing events. Ice accumulation models are in reasonable agreement to the ice thickness observed on guy wires by an onsite web camera. Icefall due to wire vibration occurs and must be accounted for in the analysis. Predictions can be improved using onsite temperature and wind speed measurements or water droplet density information from a combined analysis of onsite visibility records and cloud base observations from the airport (Harstveit et al., 2005). A rain detector with a temperature sensor can be used to detect freezing rain (Tammelin et al., 2005). However, Laakso reports a case of a rain detector that did not indicate icing even though the maintenance staff of the turbines reported freezing precipitation (Laakso et al., 2003b). Finally, ice detection based on damage analysis, such as break down of meteorological masts or power lines due to buckling or possible resonance caused by additional masses, should be an exception, but can be an additional indicator for sites where heavy icing is not expected (Seifert, 2003).

2.4 Icing evaluation during wind turbine operation

In order to use active anti-icing – de-icing system (ADIS), a reliable instrument to observe rime accretion must be available (Tammelin and Säntti, 1994). Proper and fast identification of icing events is crucial because if the heating does not start as soon as icing starts, immediate production losses follow. A reduction of power production of about 5-15% can be seen before heat is switched on (Peltola et al., 1996). Optimized ice prevention systems of wind turbines include technologies allowing proper wind speed measurements in icing conditions and reliable ice detection (Makkonen et al., 2001). The performance of a blade heating system is highly dependent on the performance of a controlling ice detector. In some

cases, several hours passed between the moment when icing could first be observed on video and the ice detector indicated icing. During this time, power production decreased considerably (Peltola et al., 2003). It has been observed that blade heating equipment receives more power than needed when there is a problem with ice detectors (Laakso et al., 2003a).

These methods for blade de-icing worked effectively, but the ice sensors used in the control systems could not reliably detect the onset of icing. A reliable icing detector is important to correctly activate the de-icing system. Detection of icing on wind turbines has different requirements than detection of icing on aircraft or for meteorological purposes (Homola et al., 2006). The ice detection must be made directly on the site (Fikke et al., 2006). Homola published a complete review of ice detection methods for operating turbines in 2006 (Homola et al., 2006). Three basic requirements for ice detection on wind turbines have been identified:

Sensor position on blade tip: Based on the icing model, the rate of ice accretion is directly related to the relative velocity of the super cooled water droplets and it is at the blade tip that the highest velocity occurs. Blade tips can experience icing due to low clouds even when the nacelle is ice-free. At Pori (Finland), measurements showed that the number of in-cloud icing periods at 84m was six times the number of in-cloud icing periods at 62m (using the relative humidity measurement method). The outer ends of the blades sweep a larger volume and collect water or ice from the entire volume. This becomes more important as the blade length increases. Because sensors are positioned on the tip of the blade near the lightning protection, it is difficult to access them in the event of failure. Also, problems associated with mounting a sensor on the blade's flexing material must be taken into account. Alternatively, the sensor can be a wireless unit for retrofitting of existing wind turbines.

High sensitivity to detect small accretion: De-icing by heating of the blades requires a much higher heating power if the airflow over the blade changes from laminar flow to turbulent flow (due to the increased heat removal of the turbulent layer). High safety risk from ice cast is already present with the accumulation of 1–2 cm of ice on the leading edge. Power production from the wind turbine is already reduced with the formation of surface roughness, with corresponding losses of income.

Ability to detect ice over a large area: Ice accumulation does not always occur at the same place on the blade. The location varies depending on the mechanisms of ice accumulation. Glaze icing can occur over large areas of the blade, with water running back and freezing away from the leading edge. Rime icing generally occurs on the leading edge, around the stagnation point, but the exact location can vary depending on the angle of attack. Also, accumulated ice can be shed from the blades. This can result in some areas of the blade having little or no ice while other areas have large accumulations. These phenomena indicate that wind turbine ice sensors should be able to detect ice at more than one or two points.

Using these criteria, 29 different methods of detection are presented in Homola's review. Here, only those that are most common in the literature are presented.

Ice detectors: This is the same technology as the one presented in the assessment section. It is also the most common method used to control the ADIS. One way to improve it could be the use of two detectors, one heated for intensity and the other unheated for duration (Tammelin et al., 2005). With slight icing, several hours can pass before icing is detected. Ice build up on blades more quickly because of their high velocity compared to static ice detectors (Laakso et al., 2003b).

Power curve errors: Comparison with normal operation power curve is used along with temperature and air pressure measurements. This analysis can be done by dividing the whole into sectors to consider the effects of wakes, topography and obstacles. A power drop of 50% is recommended as a reference for ice detection for stall regulated wind turbines. This method has the advantage of detecting icing where others fail. However, it was not possible to obtain accurate indication of ice accretion by comparing calculated and actual production power afterwards. Better results should be obtained with non-stop monitoring (Tammelin et al., 2005).

In another experiment, the operation of the de-icing system (warm air) was controlled with ice detectors and also by comparing the power output of the turbine with the expected performance that is calculated on the basis of anemometer indications (Laakso and Peltola, 2005). Power curves should be used as a safety check and always be implemented, but the difference between actual production and normal operation power curve may be explained by other factors than icing (Homola et al., 2006).

Multiple anemometry: This is the same technique as the one presented in the assessment section. The highest mounting place for an anemometer is the nacelle roof. Unfortunately, that level seems too low for detecting all in-cloud icing events at the blade tip level. In addition to this, anemometers should be seated with special care to avoid false alarms caused by the wind turbine wake effect (Marjaniemi et al., 2000).

Video monitoring: A rather good instrument for detecting ice at the rotor blades seems to be a web-cam in the hub, positioned where the pressure side of an iced rotor blade can be seen. For checking the blades' surface, in order to compare ice detection with other instruments or to check for ice accretion before a complete restart of the turbine after icing events, the web cam provides appropriate information. The disadvantage of this method is that visual observation must be continuous and requires good visibility at night, which is expensive (Seifert, 2003).

This method may be suitable for short periods of time. Although various sensors have been tested, the recording of conditions at the wind turbine using this method has not yet been conclusive for continuous ice detection, for several reasons. First, in arctic regions, there is little light during the winter. Artificial lighting is therefore needed, which can have negative visual impacts if it is in the visible spectrum. . The second and perhaps most important reason is the lack of suitable automated image analysis tools. Considering that image analysis is a fast-growing field, this type of system could become viable in the near future (Homola et al., 2006).

Vibration and noise: De-icing system operation (warm air) can be controlled with vibration sensors (Laakso and Peltola, 2005). These sensors are connected to the control system and in case of higher than normal vibrations, the turbine shuts down and blade heating starts. This method cannot detect icing during stall operation (Tammelin et al., 2005).

Another detection method for small amounts of ice accretion is the increase of aerodynamic noise coming from the rotor blades. A slim layer of ice at the leading edge increases noise and shifts the frequency to higher levels. The disturbed aerodynamic flow results in fully turbulent boundary layer from the leading edge, which produces a higher noise at a frequency that can be heard clearly (Seifert, 2003). Again, this method is not able to detect icing during stall operation (Tammelin et al., 2005). While measurement of the change in sound frequency seems to be a good indication of ice accretion, this method requires further investigation to determine how background noise and varying wind speeds affect data (Homola et al., 2006).

2.5 Recommendations

Different ice detection methods give different results. The main reasons for this are related to the fact that two different icing mechanisms are concerned: in-cloud icing due to super cooled droplets in low level clouds and freezing precipitation icing due to rain drops. Cumulative and transient effects may be significant and affect the accuracy of the predictions and, therefore, no method is accurate and reliable for all situations (Marjaniemi et al., 2000).

During Assessment Phase

To correctly evaluate icing events during the assessment phase, it is recommended to take measurements during at least one year using an ice detector, heated/unheated anemometers with heated boom, dew point and visibility detectors. It is possible for each detection method to give different information on frequency and duration of icing events. None of the ice detection methods compared here proved superior to others (Tammelin et al., 2005). Hence, the simultaneous indication of icing from at least two different sources improves prediction reliability. An ice detector is strongly recommended in conjunction with usual meteorological site measurements. Different ice detecting methods are suited to different climates and for different purposes. Different devices are needed to detect the persistency of icing and the actual icing time, the two variables that are needed to estimate ice climate. It is required to determine ice accretion period in order to determine the necessary heating energy, while the persistency of icing is necessary to determine the overall ice induced production losses. Since ice detectors are expensive for the assessment, installing one properly heated and one unheated anemometer on the measurement mast to estimate wind resource is cheap and advisable. This arrangement gives an overall picture of ice climate. Acquiring information such as time series of cloud base height from the nearest airport and comparing it with the measured data is also advisable. These two methods are likely to give a fairly good idea of the time that ice is likely to affect the operation of wind turbines. A dew point detector designed for subzero operation could also provide valuable information, because in practice, air temperature is at frost point nearly all the time when in-cloud icing occurs (Laakso et al., 2005).

During Wind Turbine Operation

A major review has been done by Homola (Homola et al., 2006) and among the 29 ice sensors, no satisfactory performance report in all conditions was found. A lot of methods, including ice collecting cylinders, dew point and temperature and double anemometry were rejected because they are mounted on the nacelle of the turbine and have limited applicability. In the event that they are modified, such that they can be mounted on the blade tip, they can be suitable and in any case they can be applicable in the absence of a blade-mounted sensor. Ice detection methods that are best suited for sensors mounted near the blade tips are infrared spectroscopy through optic fibre cables, flexible resonating diaphragms, ultrasound from inside the blade and a capacitance, inductance or impedance-based sensor. These methods were selected because they can directly measure some properties of the ice itself, they are sensitive to very thin layers of ice and they can be constructed with slight weight or no electronics near the blade tip. Among the ice detection methods used on aircraft, the ones based on capacitance and ultrasounds from within the blade seem the most suitable for wind turbines. The methods based on the resonant frequency of probes have not been shown to work successfully, perhaps due to either mounting on the nacelle or lower relative droplet velocities resulting in lower collection efficiencies than on aircraft.

3. Icing mitigation systems

Icing mitigation systems result from two main strategies: anti-icing and de-icing systems (*ADIS*). Anti-icing prevents ice to accrete on the object while de-icing removes the ice layer from the surface. Both strategies can also be divided into two methods: passive and active. Passive methods take advantage of the physical properties of the blade surface to eliminate or prevent ice, while active methods use external systems and require an energy supply that is either thermal, chemical or pneumatic (Dalili et al., 2009). Most of the strategies from the aerospace industry can be transferred to the wind energy sector, although, some scaling has to be done to adjust parameters (wind speed, chord length, airfoil) (Richert, 1996).

ADIS benefit and costs: No mass produced commercial ADIS currently exist. Although, no ADIS, passive or active, are totally effective to prevent initial and subsequent icing, during icing events some systems have proved to maintain power output, minimize dynamic impact of icing and, perhaps most importantly, avoid ice hazard close to habitable sites.

Consequently, because most ADIS are based on heating, wind turbines need more power to operate. The extra power will be added to the consumption of the nacelle cold climate package. Also, additional maintenance should be planned (Laakso et al., 2005). Tammelin et al. (Tammelin et al., 2005) concluded that the total energy consumed by WT in cold climate lies between 3 and 8% while the energy used by the anti-icing system alone is less than 3% of the total energy produced. Early studies evaluated the power consumption of ADIS electrical-heating to be 25% of the nominal power output (Makkonen and Autti, 1991), but more recent studies have lower estimates to 6 to 12% for electrical anti-icing, of 100-220kW turbines (Laakso et al., 2005) and 10 to 15% for warm air ADIS (Battisti et al., 2006). Other studies reported even lower levels, Seifert (Seifert, 2003) estimating that the heating elements consume 2% of nominal power output. In global values, the de-icing consumption translates in a 1 to 4% loss of annual energy production, depending on icing severity (Peltola et al., 2003). An investment of 5% of the cost of a 600kW turbine has been estimated for the purchase and installation of ADIS. Cost percentage decreases as turbine size increases (Laakso and Peltola, 2005). Depending on icing severity on the site (i.e. power losses related to icing) and the price of electricity, ADIS' payback time will vary from 1 to 18 years. For a site with medium icing severity, with an average of 30 icing days per year, the payback time should be less than 5 years (Tammelin et al., 2005).

Moreover, similar weather conditions may produce different icing events depending on the size of the turbine,the control strategy (stall or pitch regulated) and the operation regime (angle of attack of the blades, turning speed, etc.) (Battisti et al., 2005a). This underlines the importance of a good onsite icing evaluation for sizing ADIS.

ADIS control strategies: Most icing prevention methods are active heating systems that need a control strategy. The simplest strategy, if icing events are rare, is to continue to operate or to stop the turbine. In the second case, the turbine may be restarted automatically or after visual observation. In harsh conditions, it is recommended to use ADIS (Seifert, 2003). Another simple strategy for anti-icing system is to turn the power on all the time, but this increases energy consumption (Fortin, 2009). Usually, the ADIS basic control includes an ice detection method that turn on the system when ice is detected. If it is a heating system, more power can be delivered as the blade rotates faster, because the cooling intensity becomes higher while speed increase. Surface temperature is also a good indicator to adjust power output, avoiding overheating (Marjaniemi et al., 2000).

Anti-icing requires much more energy than de-icing because of the continuous heating. In theory, the surface temperature of the blade must be kept above $0^{o}C$ whenever there is icing.

Moreover, when ice melts on the heated elements, water can run back after the element and freeze again. To avoid this, the water must evaporate, which implies for the heated element temperature to be at least 100°C (Fortin, 2009). For de-icing systems, however, the power that is required to remove accretions already formed through rapid heating far exceeds the power required for anti-icing (Laakso et al., 2005). Icing identification must be fast to avoid power losses.

To lower energy consumption, the blade span can be divided in separately controlled sections (Maissan, 2001). Because of low relative wind speed and smaller contribution to power production, the first two-thirds of the blade is less important to de-ice, and therefore requires less energy. Setting up a de-icing system only on the last third of the blade would enable to decrease equipment and energy costs while maintaining 90% of the aerodynamic performance of the clean blade with only 30% of the length de-iced (Hochart et al., 2008). The tip, however, must be as clean as possible. The use of heating resistance allows a more efficient energy distribution on the blade, which is particularly difficult to achieve with a hot air system (Mayer et al., 2007). For mechanical systems, a minimal ice layer thickness is required, and thin layers formed on the leading edge are harder to remove. It has been proposed to combine a heated element on the leading edge with a mechanical system elsewhere (Fortin, 2009).

3.1 Passive Anti-Icing and De-Icing Systems (ADIS)

The passive anti-icing systems are: special coating, black paint or chemicals. The characteristics, advantages and inconvenient of each system are presented here.

Special coating: In theory, ice-phobic coatings prevent ice from sticking to the surface because of their anti-adherent property, while super-hydrophobic coatings do not allow water to remain on the surface because of repulsive features. Reducing the shear forces between the ice and the surface will also reduce sensitivity to dirt and bugs (Seifert, 2003). Currently, most manufacturers use epoxy or polyester matrix composites reinforced with glass and/or carbon fibres, although polyester and glass fibres remain the material of choice due to their lower cost. Current research is heading towards nanocomposite coatings, polymers reinforced by minute, nanometre-scale particles. These nano-composites create very high contact angles with water (Dalili et al., 2009). A combination of coatings and active ADIS should be considered for preventing ice accretion (Kimura et al., 2003).

The advantages of the special coating are: low cost, no special lightning protection required, easy blade maintenance and a protection of the whole surface (Seifert, 2003). The reduction of ice adhesion combined to a blade heating system should lower energy consumption. The most effective coatings were found to reduce the adhesion of ice to about half of what is observed on uncoated aluminum (Anderson and Reich, 1997). The adhesion strength of accreted ice is reduced when blades are treated with the appropriate coating (water-repellent agent) (Kimura et al., 2003). A single application of coating material could provide a multipurpose solution that may reduce the frequency of unscheduled shutdowns and maintenance issues (Dalili et al., 2009).

However, the icing prevention on wind turbine blades by coating alone is not realistic. Several materials have been lab and field-tested but no adequate solution has been found. Icing occurred even on coated surfaces, regardless of the temperature (Kimura et al., 2003). None of the coatings was found to be truly ice-phobic (Anderson and Reich, 1997). Other disadvantages are the ice throw, the large accretion during severe icing and the unsymmetrical accretion leading to instability (Seifert, 2003). After a short period, the

coating becomes porous and loses its ability to repel ice (Tammelin et al., 2000). Detailed information for most of these coatings remains proprietary. Consequently, most data sheets and chemical compositions are classified and inaccessible (Dalili et al., 2009).

Black paint: Black paint allows blade heating during daylight and is used with an ice-phobic coating. When tested in Yukon (Canada), this method showed immediate and noticeable improvement in performance (Maissan, 2001). This method may be sufficient in sites where icing is slight, infrequent and where icing periods are followed by temperatures above 0°C or in areas with high winter solar intensity at lower altitudes (Laakso et al., 2003a). Most of the time, it is not sufficient to prevent icing (Laakso et al., 2005). Temperature of the blade's surface may affect the properties of glass-fibre reinforced plastics, as they are sensitive to high temperature (Seifert, 2003). However, another study shows that black blades do not overheat in the summer (Weis and Maissan, 2003).

Chemicals: When applied on blade surface, chemicals lower the water's freezing (Patreau et al., 1998). It is mostly used during aircraft take-off. It is a pollutant and it needs special application and a lot of maintenance (Patreau et al., 1998). It cannot remain on the surface of the blade for a long period (Tammelin et al., 2000).

The passive de-icing systems are: *flexible blades* and *active pitching*. *Flexible blades* are flexible enough to crack the ice loose. Blade flexing is known to help shed the ice but very few information is available on the subject (Dalili et al., 2009). The *active pitching* is a semi-active method that uses start/stop cycles to orient iced blades into the sun (Laakso et al., 2005). The method may work in slight icing environments but it has not been scientifically validated and may damage wind turbines (Laakso et al., 2005).

3.2 Active Anti-Icing and De-Icing Systems (ADIS)

Anti-Icing Systems: The active anti-icing systems are used to prevent the ice accretion on blade surface and are based on resistive, air layer or microwave heating. Heating resistance and warm air can be used in anti-icing mode to prevent icing. The blade temperature should be kept around 0°C to prevent icing. The advantage is that no ice accumulates on blades. Blade can be kept at -5°C, instead of 0°C, in good condition. This way, 33% of power can be saved which represents 2.3% of winter production (Mayer, 2007). The inconvenient is that it requires a lot of energy. If it is used to prevent runback at 100°C, it is close to the softening point of some epoxies and resins (although thermosetting plastics that are designed for higher operating temperatures are available). The continuous operating temperature should be less than 50°C with current blade materials (Laakso and Peltola, 2005). The air layer consists in an air flow originating inside the blade and pushed through rows of small holes near the blades' leading and trailing edges in order to generate a layer of clean and, if necessary, heated air, directly around the blade surface (Dalili et al., 2009). This method would deflect the majority of water droplets in the air and would melt the few droplets that managed to hit the surface but very few information is available for its application (Dalili et al., 2009). Microwave heating consists in heating the blade's material with microwaves to prevent ice formation. The objective is to maintain the blade surface at a temperature slightly above 0°C, in order to save up some energy that will be used for defrosting. It is recommended to cover the surface of the blade with a material that reflects microwaves (metallic material such as wire mesh) and apply paint to improve the final surface. Another method consists in heating the blades when they pass in front of the tower by fixing an emitter on the tower. (Mayer, 2007). It has been tested at the LM Glassfiber workshop on a

LM19.1 blade with a 6kW power, a frequency of 2.45GHz and an emitted power less than 0.01W/m2 but is still to be implemented commercially (Mansson, 2004).

De-Icing Systems: The active de-icing systems are used to eliminate the ice accreted on the blade using a heating resistance, hot air, flexible pneumatic boots and electro impulsive/expulsive devices.

Heating resistance: The electrical heating uses an electrical resistance embedded inside the membrane or laminated on the surface (Laakso et al., 2005). The idea is to create a water film between the ice and the surface. Once this film created, centrifugal forces will throw the ice away (Battisti et al., 2006). Electrically heated foils can be heating wires or carbon fibres (Seifert, 2003). Heating elements cover the leading edge area of the blade. The ice detector and blade surface temperature are used to control the operation of the heating system. Additional temperature sensors are installed to protect the blade from permanent damage induced by over-heating. Heating foil can be applied to most turbines (Tammelin et al., 2005). For the Finnish JE-System, the estimated heating power to keep the total blade area rime and ice free is around 1.2kW/m (Tammelin and Säntti, 1994). Most recent results have proved to be about 0.5kW/m, which represents 5% of the wind turbine rated power (Marjaniemi and Peltola, 1998). A system of 15kW per blade has been used for a 600kW wind turbine, corresponding to 1-4% of annual production, depending on climate conditions (Laakso and Peltola, 2005). A system installed on a 1.8 MW turbine will needs 82kW per blade or 14% of power output at 8m/s (Mayer, 2007). Another system was tested using about 3.4kW per blades on small Bonus 150kW turbines (Pinard and Maissan, 2003). The minimum time to keep the heating on, after the icing event has passed, is usually about 15-30min (Peltola et al., 1996). Heating demand is almost linearly dependent on the temperature difference between the air and the blade surface (Marjaniemi and Peltola, 1998). More energy is needed to de-ice the tip's leading edge than the hub's (3.5 to 3.9 times more). More energy is also needed to de-ice the tip's trailing edge than the hub's (2.6 to 2.9 times more) and to de-ice the lower surface rather than the upper (1.3 to 1.5 times more) (Mayer et al., 2007). This simple method has been used successfully in the aerospace industry for many years. It has also been also used in the wind industry since 1990 (Dalili et al., 2009). JE Finnish's equipment is the most used and is installed on 18 wind turbines (Laakso and Peltola, 2005; Makkonen et al., 2001). The needed heating energy during rime accretion is quite small considering the profitability of wind energy production (Tammelin and Säntti, 1994). Heating power seems to be adequate except in the case of super cooled rain (Marjaniemi and Peltola, 1998). Thermal efficiency is close to 100% because of direct heating (Battisti et al., 2005a). Energy demand does not increase with blade size (Laakso and Peltola, 2005). As an inconvenient, there are many commercially available products but none are mass produced (Dalili et al., 2009). The technology is still at the prototype level because of the limited market (Laakso et al., 2005). If one heater fails, it will cause major imbalance on the whole system (Maissan, 2001). In some extreme icing cases, blade heating power was found to be insufficient (Peltola et al., 2003). Icing of the run-back water at the edges of the heating elements occurs quite often. When the running water from the heating element area reaches a cold blade surface, it re-freezes and forms a barrier at the edges of the heating element. The edge barriers may grow towards the leading edge as "horns" without a contact with the heating element. This could explain why in some blade icing cases, the thermostat of the ice prevention system indicates a temperature higher than 0°C on the surface of the heating element during icing (Makkonen et al., 2001). Heating elements can attract lightning

but lightning protection is efficient and no damage was detected in the ice prevention system studied by Marjaniemi (Marjaniemi et al., 2000).

Hot air: The second method consists in blowing warm air into the rotor blade at standstill with special tubes (Seifert, 2003). Blowers located in the root of each blade or inside the hub produce the hot air. The heat is transferred through the blade shell in order to keep the blade free of ice (Laakso and Peltola, 2005). Again, the idea is to develop a water film between the ice and the surface. Once developed, it allows centrifugal forces to get rid of the ice (Battisti et al., 2006), but heating is also possible during parking (Laakso and Peltola, 2005). An air circuit is created inside the blade by dividing the internal volume in two parts. Hot air is injected in one part, which sends the cold air to the heating system on the other section (Mayer, 2007). Using a closed circuit, heating power is reduced significantly compared to an open cycle where air needs to be heated to the desired temperature starting from the outside temperature. Efficiency can be improved by using waste heat from the machinery (Peltola et al., 2003). A prototype is installed on an Enercon turbine in Switzerland and consists in a 7kW hot air blower in each rotor blade for a 850kW wind turbine. It consumes 1% of the total electricity production (Horbaty, 2005). Relatively low temperatures of the warm-air (80–120 °C) are suitable for the de-icing process, allowing lower temperatures (60–80 °C) of the blade surface, compared with the anti-icing practice (Battisti and Fedrizzi, 2007). The leading edge surface and the blade's aerodynamics are not affected. The system has no negative effect on the lightning protection system (Seifert, 2003). It works well in milder climates where icing occurs mainly at temperatures close to 0°C (Laakso et al., 2005). De-icing systems have a substantial advantage over anti-icing systems in terms of energy consumption: the energy consumption ratio is 50% for all simulations (Battisti et al., 2006). One inconvenient of the method is that it uses a lot of power at high wind speed and low temperature. Also, glass-fibre reinforced plastics (GRP) material is a good insulator and, as blades increase in size and thickness, more heat needs to be pushed and transferred trough the surface and to the tip of the blade (Seifert, 2003). The maximum operating temperatures of composites must be considered (Laakso et al., 2005). As this system works once the ice is accreted, there is a safety hazard related to ice projection. Thermal efficiency is low (about 30%) (Battisti et al., 2005a). The thermal efficiency of closed loop hot air based system will remain rather poor, because large mass of material has to be heated prior to attending the blade surface. Also, the heat source, often a hot air blower, is located typically at the blade root while the highest heat fluxes are needed at the tip of the blade (Laakso and Peltola, 2005).

Flexible pneumatic boots inflate to break ice. In the normal non-inflated state, tubes lay flat and are attached to the airfoil surface on which the de-icer is bonded. After the build up of generally 6 to 13 mm of ice on the surface of the airfoil, de-icers are inflated with compressed air. The inflation cycle lasts for a few seconds to achieve optimal ice shed and prevent additional ice formation on the inflated surface. After the ice has cracked, its bond to the surface is broken and it is removed through centrifugal and aerodynamic forces. De-icers are then allowed to deflate. Vacuum is then applied to ensure that there is no lifting of the surface on the low-pressure side of the airfoil (Botura and Fisher, 2003). Goodrich has tested this method in laboratory. Three 6 by 1m de-icers where tested on a simulated 1.5MW wind turbine rotor blade. De-icers for wind turbine applications have equivalent ice shedding and residual ice performance as conventional aircraft de-icers. Working at higher pressures for wind turbine applications, tests indicated satisfactory icing shedding on glaze ice at temperatures above -10ºC and residual ice at temperatures between -10 and -20ºC.

During in-field operation, residual ice is reduced due to blade vibration and centrifugal forces (Botura and Fisher, 2003). The system is installed on many aircrafts and has low energy consumption (Mayer, 2007). However, the method has yet to be field-tested for wind turbine application. The test is currently on hold pending agreement with a suitable wind turbine manufacturer or operator (Botura and Fisher, 2003). It may disturb the aerodynamics by increasing drag and cause more noise. Ice expulsion is a potential problem. During the 20 years of operation, it will require intensive maintenance, which may be expensive. High centrifugal loads at the outer radius of the pneumatic system will inflate itself or has to be divided in short sections (Seifert, 2003).

Electro impulsive/expulsive devices: This consists in very rapid electromagnetically induced vibration pulses in cycles that flex a metal abrasion shield and crack the ice (Dalili et al., 2009). A spiral coil is placed near the surface of the blade. When current is applied to the coil, a magnetic field is created between the coil and the thickness of the blade. The result is a rapid movement of the surface and the expulsion of the accumulated ice (Mayer, 2007). The method has been recently certified for use on Raytheon's Premier I business jet (Dalili et al., 2009). It is used by Hydro-Quebec for transmission lines and Goodrich is currently developing this method for aeronautical applications. The system is efficient, environmentally friendly, has low energy consumption, causes no interference with Hertz transmission and is easily automated (Mayer, 2007). In the mean time, it is a new technology that has not yet been tested on wind turbines. Ice expulsion is a potential problem (Mayer, 2007).

3.3 Synthesis and conclusion of existing methods for evaluation and mitigation of ice accretion on wind turbines (literature review)

Considering the current available technology, the following recommendations can be made for wind turbines exposed to icing and for the use of ADIS.

Icing assessment with multiple anemometry and relative humidity: double anemometry is a proven way to estimate onsite icing. As opposed to icing sensors, anemometers are cheap and have low energy consumption, which is a great advantage for remote site met masts. Triple anemometry seems a promising way to measure the severity and the duration of icing (Craig and Craig, 1996). Relative humidity or dew point detectors are also a cheap way to detect clouds and can identify icing for temperatures below 0°C. As this method is not reliable on its own (Tammelin et al., 2005), combining it with multiple anemometry seems ideal for assessment. Another way to detect clouds is video monitoring, but this method has yet to be automated.

Icing detection by ice sensors and power curve check during operation: ice sensor methods are currently the only proven way to directly measure icing during operation. It is also the most used method for current ADIS. Unfortunately, this method has several disadvantages. The most important one is that measurements are made at the nacelle level (Dalili et al., 2009). Combining this method with power curve checks can improve accuracy. Methods currently being developed, including capacitance and infrared stereoscopy, will be able to measure icing on several blade points (mainly close to the tip) with great precision (Dalili et al., 2009).

Passive method of special coating with active heating elements: This is the only method currently available and it has been tested for more than 20 years. This method is simple and its efficiency is close to 100% because it involves direct heating of the blades. It requires a large amount of energy that can be reduced through different strategies. First, a better control strategy that properly uses de-icing instead of anti-icing. Second, as detection methods improve, heating will be more efficiently started. Third, a combination with special coating

will reduce adhesion of ice and run-backs. New developments in special coating will help reduce the energy demand. The warm air method will be more difficult to use with larger blades. Commercially produced anti-icing or de-icing systems have not yet been proven reliable and there have been reports on damage of prototype heating systems. Therefore, some manufacturers prefer using special coatings of the blade's surface instead of heating systems (Seifert, 2003).

4. Experimental analysis of wind turbine icing and optimization of electro-thermal de-icing

The wind farm near Murdochville, Quebec, is a good example of the severe effects of cold climate on wind turbines. The farm has 60 Vestas 1.8 MW turbines and is located between 850 and 950 m altitude. During the 2004-05 winter and spring, the meteorological station operated at 610 m altitude by the Wind Energy TechnoCentre, located near the wind park of Murdochville, recorded 13 icing events (Fortin et al. 2005a). Among these 13 events, five were considered severe and a hazard for the wind farm. Two events out of the five were selected for wind-tunnel simulation to study their effects on the Vestas-V80 wind turbine, through a quantitative study of ice-accretion shape, lift reduction and drag increase. The two icing events selected for the simulations were in-fog icing conditions as shown in Table 1. They were characterized by their liquid water content (LWC), median volume diameter (MVD) of the super cooled droplets, air speed (V_∞), air temperature (T_∞), and duration of the event (t):

Event	LWC (g/m³)	MVD (μm)	V∞ (m/s)	T∞ (°C)	T (min)
1	0.218	38.3	8.8	-1.4	360
2	0.242	40.5	4.2	-5.7	264

Table 1. Characteristics of measured icing events used for wind-tunnel simulation of in-fog icing (Fortin et al. 2005a)

The tests were carried out in the AMIL (Anti-icing Materials International Laboratory) icing wind tunnel (IWT) at the Université du Québec à Chicoutimi (Figure 1). It is a refrigerated closed loop wind tunnel 4.5 m wide and 9.5 m long. The test section is 0.6 m high, 1.5 m long and 0.5 m wide. The working temperature range is -30 °C to +25 °C. The maximum wind speed is 70 m/s.

In-fog icing is produced using an oscillating spray-nozzle assembly located upwind from the convergent. The spray nozzles are set to produce water droplets with a diameter of 27.6 μm. The lift and drag forces are measured using an aerodynamic scale made up of two aluminum arms linked together by a bearing. A load cell is placed at the end of each arm to record the lift and drag forces on blade airfoil in the test section.

Generally, the shapes of ice deposits used in wind-tunnel aerodynamic simulations are measured directly on blades during icing events, or calculated by ice-accretion simulation software. An artificial deposit is then moulded and glued along the blade profile to simulate the 2D runoff on an iced blade profile. Seifert and Richert (Seifert and Richert, 1997) presented experimental measurements of lift and drag on a blade airfoil, the leading edge of which was covered with artificial ice deposits shaped from actual deposits collected from a small, horizontal-axis wind turbine during different icing periods. Jasinski (Jasinski et al., 1997) made the same measurements, but used artificial ice shapes created with the LEWICE

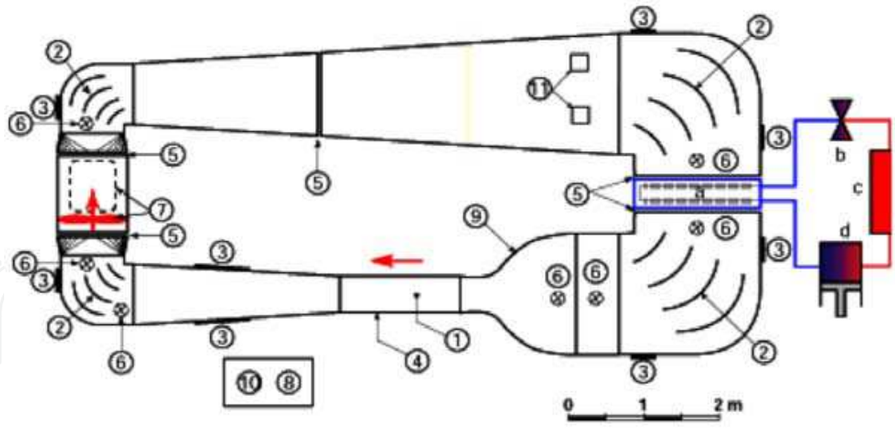

1	Test section	9	Contraction cone
2	Corner vanes	10	Control console
3	Access doors	11	Traps
4	Access panels	a	evaporator
5	Thermal expansion joints	b	Expansion valve
6	Spray nozzle ramp	c	Condenser
7	Fan and Motor	d	Compressor
8	Motor control panel		

Fig. 1. The AMIL Refrigerated Wind Tunnel (Hochart et al. 2008)

ice-accretion simulation software at NASA. The special feature of the experiments described here (Hochart et al. 2008) resides in the way the ice deposits on the blade airfoil was obtained by simulating in a wind tunnel the meteorological and operating conditions of the wind turbine during in-fog icing. The effects of ice accretion were determined in two phases: one phase of ice-accretion when the shape has been determined and a second phase to determine the aerodynamic characteristics (lift and drag) of the iced airfoil. A load calculation based on the blade element theory [Burton et al. 2001] was used to estimate the effects of icing on the driving and bending forces, as well as torque. The resulting data were used as a basis to determine the power loss and the best position for the heating-element of a de-icing system.

A second analysis was done to establish the de-icing parameters in order to optimize the heating process and minimize electric energy consumption. The calculation of the power used for the de-icing is based on the evaluation of the convective heat transfer on the airfoil surface. The experimental study quantifies the power consumption for the whole icing event as well as the evolution of the surface temperature and heating.

The Vestas-V80 wind-turbine blade uses a NACA 63 XXX airfoil between the blade tip and its centre, and a FFA W3 XXX airfoil between the centre of the blade and the hub (Anonymous, 2004). Because the exact blade airfoil configuration was unknown, a 0.2 m (chord) x 0.5 m (width) NACA 63 415 airfoil was chosen for testing. The model for the analysis of ice accretion shape was cut from a block of 6061-T6 aluminum, has a 200 μm

surface finish and was horizontally mounted, suction side upwards, in the test section (Figure 3a). The blade section used for the analysis and optimisation of de-icing system is made with fibreglass tissue as close as possible to that of the real blades. Considering its size, the fibreglass tissue layers of the blade section follows the orientation [±45°/0°/±45°] (McKittrick et al., 2001). Consequently, the thickness of fibreglass is approximately 1.96 mm along the airfoil. It is equipped with 12 resistant heating elements and instrumented with 12 thermocouples (Figure 3b).

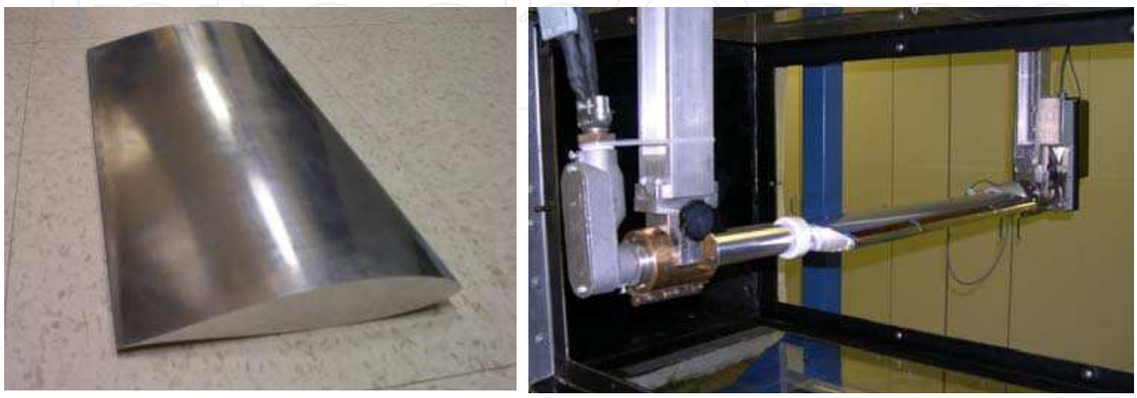

(a) (b)

Fig. 2. (a) Blade Sections for Ice Accretion and (b) De-Icing Analysis (based on NACA 63-415 airfoil) (Hochart et al., 2008, Mayer et al. 2007)

5. Experimental evaluation of icing effect on the wind turbine performance

5.1 Test cases

To determine the effect of ice accretion at different span positions across the blade, the cinematic conditions have been simulated at three radial positions, 12 m, 23.5 m and 35 m, of the 40 m blade. Each simulation included two major parameters, the relative wind speed (V_{rel}) and the angle of attack (α). As shown in Figure 3, these parameters were calculated from the wind speed at the rotor disc entrance (V_{vent}), the tangential speed (V_{tang}) and the pitch angle (φ).The relative wind speed was:

$$V_{rel} = \sqrt{V_{vent}^2 + V_{\tan g}^2} \tag{2}$$

and the angle of attack (α) was:

$$\alpha = \arctan\left(\frac{V_{vent}}{V_{\tan g}}\right) - \varphi \tag{3}$$

The wind speed at the rotor disc entrance (V_{vent}) was calculated using the actuator disc concept (Burton et al., 2001),

$$V_{vent} = V_{\infty}(1-a) \tag{4}$$

and the tangential speed (V_{tang}) of the blade section was derived from the rotor disk theory (Burton et al., 2001):

$$V_{\text{tang}} = \omega r(1 + a') \tag{5}$$

The axial induction factor, a, was assumed to be 1/3. This is an optimal value for the wind turbine power coefficient (C_p), according to the actuator disc concept. The radial induction factor was assumed to be very small (a' << 1) and tip corrections were not included. The twist angle was calculated for an optimal lift to drag ratio along the blade with a free stream speed (V_∞) of 8 m/s. These assumptions, as explained in the blade element theory (Burton et al., 2001), are usually good approximations for fairly well designed wind turbines in normal conditions (without ice). Therefore, they were considered as acceptable to the aim of this work, which is not to accurately calculate air flow or aerodynamic forces along the blade but only to emphasize the difference between iced and non iced situations.

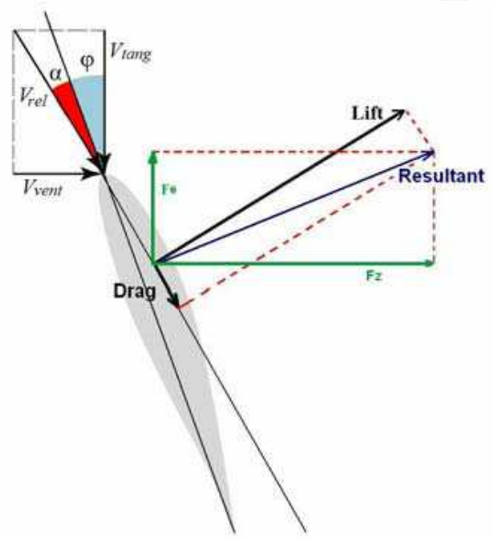

Fig. 3. Cinematic of the blade section (speed and angle of attack)

The meteorological conditions for the two in-fog icing conditions selected were scaled down to wind-tunnel dimensions. The method described by Anderson (Anderson, 2004) was used. The fixed variables for scaling were the model chord, 0.2 m, and the median volume diameter (MVD) of the water droplets, 27.6 μm. The imposed variable was the air speed in the wind tunnel, which corresponds to the relative air speed at the radial position tested. The free variables were the liquid water content, air temperature, and duration of the event. The simulation parameters for the six tests are shown in Table 2. They are the radial position (r), angle of attack (α), liquid water content, median volume diameter of the supercooled water droplets, relative air speed (V_{rel}), experimental Reynolds numbers (Re), wind-tunnel temperature (T_∞), and duration of the event (t).

The liquid water content (LWC) was calibrated using the rotating cylinder method (Stallabrass, 1978), which consists in accreting ice on a rotating cylinder of 5 cm diameter during one hour. The spray nozzles were adjusted to yield, at a given speed, the desired liquid water content. The experimental method for the simulations consisted in positioning the blade airfoil (Figure 2a) at the desired angle of attack; setting the speed, temperature, and liquid water content in the test section; accreting ice on the airfoil for a specified duration; measuring the lift and drag coefficients; weighing the blade profile to determine

the mass of accreted ice; and draw the ice shape at the centre of the blade section. Each simulation was repeated once to ensure conformity of results.

Test	Fog	R (m)	α (°)	LWC (g/m³)	MVD (μm)	V_{rel} (m/s)	Re	T∞ (°C)	T (min)
1	1	11.9	13	0.37	27.6	19.9	2.65×10^{05}	-1.4	14.8
2	1	23.4	13	0.48	27.6	38.0	5.07×10^{05}	-1.4	15.1
3	1	34.8	13	0.48	27.6	56.0	7.47×10^{05}	-1.4	24.8
4	2	11.8	3	0.37	27.6	18.7	2.49×10^{05}	-5.7	10.6
5	2	23.3	7	0.48	27.6	36.7	4.89×10^{05}	-5.7	11.8
6	2	35.0	9	0.48	27.6	55.0	7.33×10^{05}	-5.7	19.6

Table 2. Wind-tunnel simulation parameters

5.2 Results

The results of the six simulations for ice mass, ice-deposit shape, lift reduction and drag increase are described in this section.

In-fog icing event 1

Tests 1 to 3 simulated the effects of in-fog icing event 1 on three positions of a Vestas 1.8 MW wind-turbine blade. The icing event characteristics were as follows: LWC of 0.218 g/m³; temperature of -1.4 °C; wind speed of 8.8 m/s; duration of 6 hrs. For this wind speed, the angle of attack was calculated to 13° for all simulations. Simulations 1, 2, and 3 correspond to 11.9 m, 23.4 m, and 34.8 m span positions from the hub, respectively.

Figure 5a shows the masses and shapes of the ice deposits for simulations 1 to 3 of in-fog icing 1. For the three simulations, the deposits on the blade were glaze, a transparent ice of high-density (917 kg/m³) characteristic of wet-regime accretions. A fraction of the water striking the leading edge of the blade profile froze upon impact while the rest ran along the pressure surface and, at very high speeds, along the suction surface as well. All or some of the running water may freeze on the pressure and suction surfaces of the blade airfoil.

Figure 5b shows the lift coefficient reduction and the drag coefficient increase for wet-regime simulations 1, 2 and 3. The lift coefficients measured on the iced profiles were 0.697, 0.685 and 0.553 for the simulations corresponding to radial position 11.9 m, 23.4 m and 34.8 m respectively. The drag coefficients measured for the same simulations were 0.068, 0.090, and 0.195 respectively.

The unfrozen water flowed to the trailing edge where some of it froze and the rest sprayed off into the air. Moreover, because of the sharp angle of attack, some droplets struck the pressure surface, thus increasing the water flow. In the ice accretion simulation near the hub (Figure 6a), the glaze on the leading edge followed the contour of the blade profile. In the ice accretion simulation near the middle of the blade (Figure 6b and Figure 6c), the glaze on the leading edge and that on the pressure surface followed the contour of the blade profile. In the ice accretion simulation near the blade tip (Figure 6d), the glaze on the leading edge was horn shaped, on the pressure side followed the contour of the blade profile, while on the suction side formed rivulets. The glaze on both sides of the airfoil was the result of runoff water that froze nearly completely for the simulation near the hub, and partially for the simulations near the mid and tip positions. For these last two positions, a fraction of the runoff water froze on the trailing edge. The quantities of captured water and glaze increased

with an increase in the relative air velocity seen by the blade section. The ice masses experimentally accreted on the blade section in the tunnel were 48 g, 130 g and 354 g for the simulations corresponding to radial positions 11.9 m, 23.4 m and 34.8 m respectively.

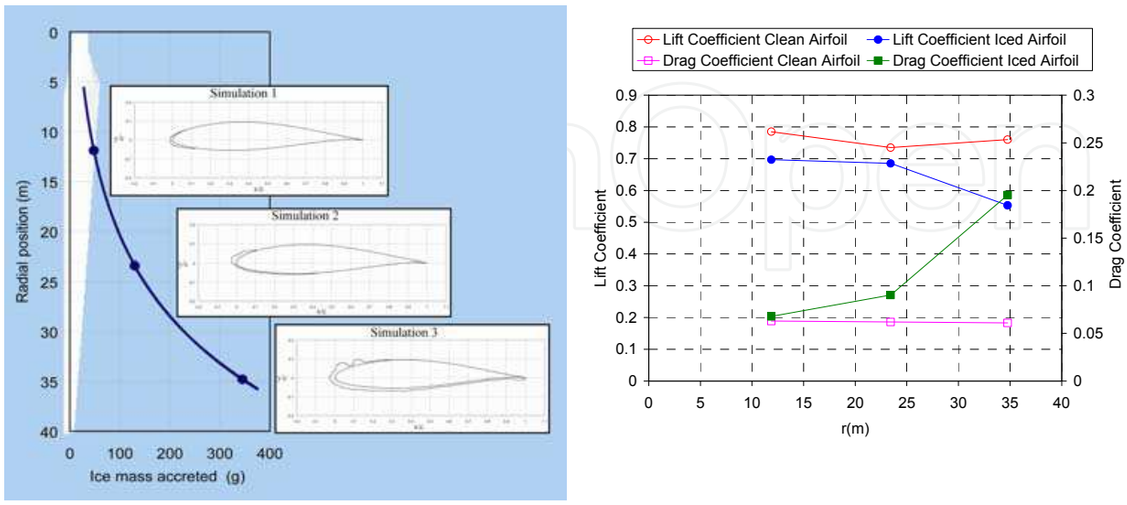

Fig. 5. (a) Masses and shapes of ice deposits for icing event 1 and (b) Lift and drag coefficients for icing event 1

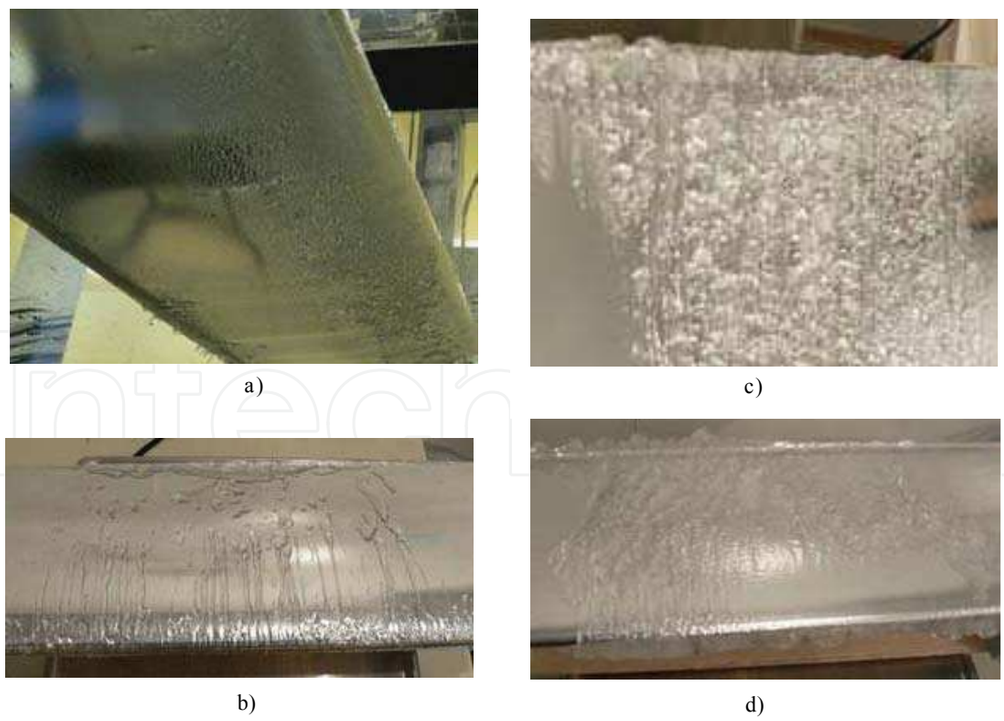

Fig. 6. Iced blade shape at the end of the simulations, a) simulation 1, view from below, b) simulation 2, view from above, c) simulation 2, view from below, d) simulation 3, view from below

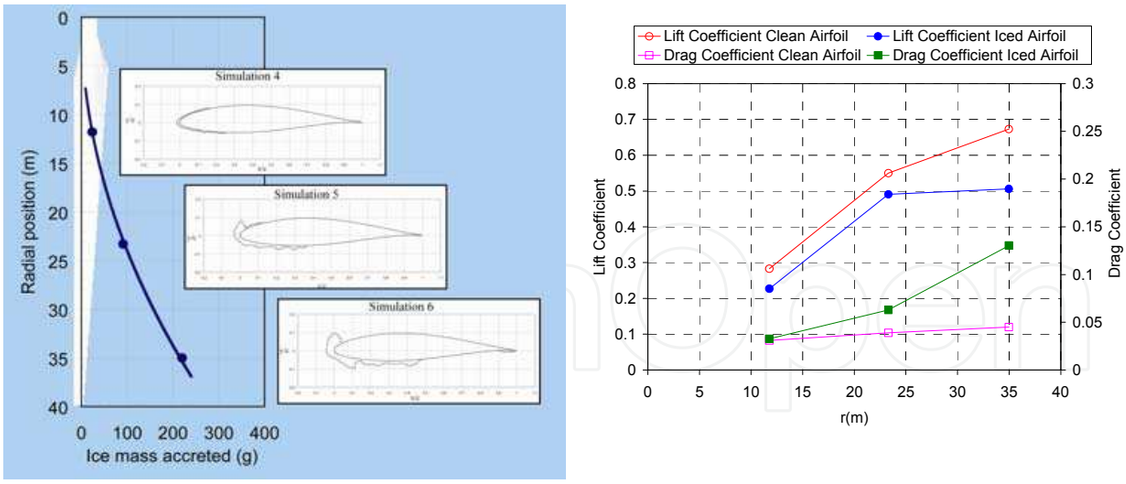

Fig. 7. (a): Masses and shapes of ice deposits for icing event 2 and (b): Lift and drag coefficients for icing event 2

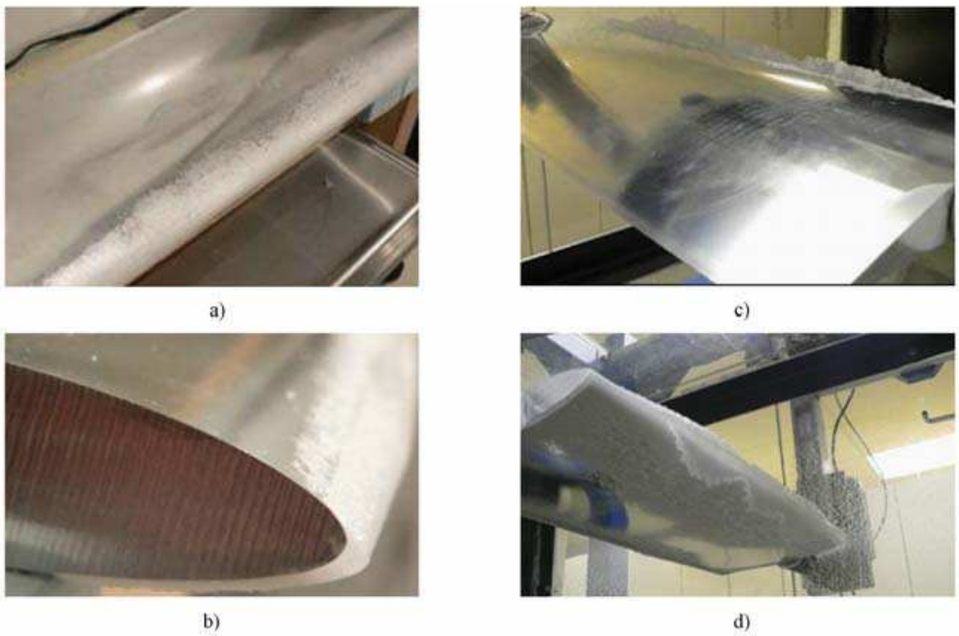

Fig. 8. Iced blade profiles at the end of the simulations, a) simulation 4, view from below, b) simulation 5, side view and from below, c) simulation 6, view from above, d) simulation 6, view from below

All the water striking the leading edge and the blade profile froze upon impact. For the simulation corresponding to the cross section closest to the hub (Figure 8a), the rime on the leading edge, pressure surface, and suction surface partially followed the contour of the blade profile and formed slight protrusions. For the cross section near the middle of the blade (Figure 8b) and closest to the tip (Figure 8c and Figure 8d), the rime on the leading edge had a double-horn shape, and that on the pressure and suction side partially followed the contour of the blade profile and exhibited protrusions. The rime was oriented in the

direction of the water droplets incidence angle, creating zones of shadow with little accretion, leading to the formation of protrusions. The quantity of accreted rime increased with an increase in the relative air velocity seen by the blade section, due to the proportional increase of captured water, as follows: 24 g, 91 g and 220 g for the simulations at radial positions 11.8 m, 23.3 m and 35 m respectively.

5.3 Analysis

The dry-regime simulations (icing event 2) were easier to carry out than those in wet regime (icing event 1) because they have better reproducibility. Each simulation was repeated once. Tables 3, 4 and 5 show the mean values and the standard deviations of ice mass, lift coefficient and drag coefficient for the two simulations carried for each regime. Standard deviations are based on the two average values measured during the experiments and not on the signals in time.

Icing Event	Wet Regime (Event 1)			Dry Regime (Event 2)		
Radial Position(m)	11.9	23.4	34.8	11.8	23.3	35.0
Average mass of ice (g)	48	130	354	24	91	220
Standard Deviation(g)	0.25	9.25	4.5	1.75	0.25	5.5
Standard Deviation (%)	0.52	7.07	1.27	7.36	0.28	2.5

Table 3. Average values and standard deviations of ice mass

Icing Event	Wet Regime (Event 1)			Dry Regime (Event 2)		
Radial Position(m)	11.9	23.4	34.8	11.8	23.3	35.0
Average Lift Coefficient	0.697	0.685	0.553	0.227	0.491	0.226
Standard Deviation	0.021	0.011	0.088	0.004	0.012	0.016
Standard Deviation (%)	3.04	1.54	15.9	1.87	2.39	3.2

Table 4. Average values and standard deviations of lift coefficient

Icing Event	Wet Regime (Event 1)			Dry Regime (Event 2)		
Radial Position(m)	11.9	23.4	34.8	11.8	23.3	35.0
Average Drag Coefficient	0.068	0.09	0.195	0.033	0.063	0.13
Standard Deviation	0.01	0.017	0	0.0026	0.0017	0.009
Standard Deviation (%)	14.7	18.4	0	7.9	2.8	6.9

Table 5. Average values and standard deviations of drag coefficient

As shown in Figures 5a and 7a, in both wet (icing event 1) and dry (icing event 2) regimes, because of local cinematic conditions, the ice mass accreted on the airfoil increases as the cross section moves from the hub to the blade tip. In order to show dimensionless results (Table 6), the accreted ice masses on the experimental blade airfoil have been revaluated for the six simulations considering a standard 1 m (chord) x 1 m (width) NACA 63 415 airfoil and the six ice shapes of Figure 5 and Figure 8. For a real blade, the chord length decreases with the radial position from the hub to the blade tip. Considering this size variation, it is in the median zone of the full size blade that the largest quantity of ice accretes, as shown in Figure 9. The total mass of accreted ice is estimated to 709 kg for event 1 (11% of the blade initial mass, which is 6500 kg) and 434 kg for event 2 (6.7% of the blade initial mass).

Icing Event	Wet Regime (Event 1)			Dry Regime (Event 2)		
Radial Position(m)	11.9	23.4	34.8	11.8	23.3	35.0
Average mass of ice (g)	2400	6500	17700	1200	4550	11000

Table 6. Average values of ice mass, dimensionless 1 m (chord) x 1 m (width) profile

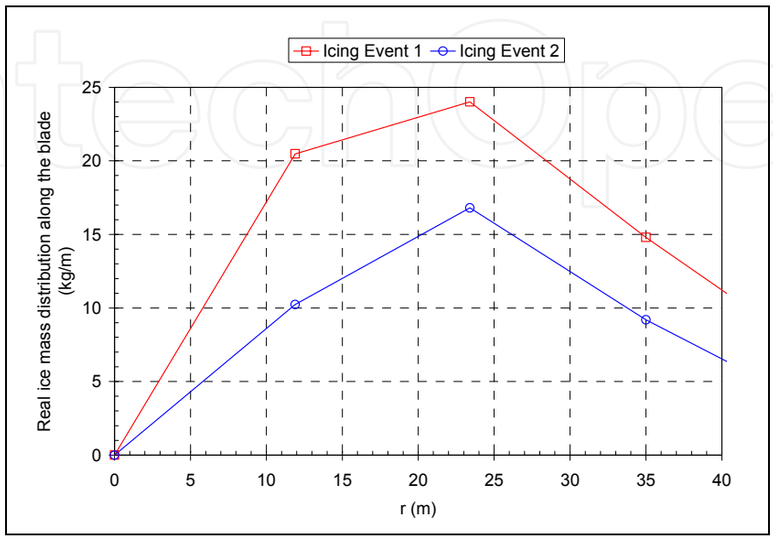

Fig. 9. Mass of ice accumulated along the full size rotor blade

In both dry and wet regimes, the lift and drag coefficients are more affected as we move from the hub to the blade tip. In Figures 7 and 10 it is illustrated how the lift coefficient decreases and drag coefficient increases with the radial position on the blade. The drag coefficient variation with radius follows approximately a power law. Especially between the middle and the blade tip, drag coefficient increased considerably and, combined with lift decreases, lead to a significant reduction of lift to drag ratio. In wet regime (icing event 1), we estimated that drag coefficient increased 7.7 % at 11.9m, 45.7 % at 23.4 m and 220 % at 34.8 m, according to the test results corresponding to the respective positions on the real blade. Using the same assumptions, the lift coefficient decreased 11.2 % at 11.9 m, 6.8% at 23.4 m and 27.2 % at 34.8 m. The drag coefficient increase at the blade tip (40 m) is estimated to 365% and the lift coefficient reduction to 40 %. In dry regime (icing event 2), drag coefficient increased 5.5 % at 11.8 m, 61.3 % at 23.3 m and 190 % at 35.0 m, according to the test results corresponding to the respective positions on the real blade. Lift coefficient decreased 19.8 % at 11.8 m, 10.7 % at 23.3 m and 24.8 % at 34.8 m. The drag coefficient increase at the blade tip (40 m) was estimated to 250 % and the lift coefficient reduction to 37%.

In order to assess the effect of ice on the aerodynamic forces on the full size rotor, a load calculation based on the blade element theory (Burton et al, 2001) has been used. The orthoradial force component, which generates rotor torque, is called driving force and noted as F_θ. The force component perpendicular to F_θ, noted as F_Z, is oriented in the direction of the rotor axis and serves to estimate the bending force applied to the blade. The formulas for dF_θ and dF_z are:

$$dF_\theta(r) = \left(\frac{1}{2}\rho\, c(r)\, \sqrt{V_{vent}^2 + r^2\omega^2}\right)\left(C_L(r)V_{vent} - C_D(r)\,\omega r\right)dr \tag{5}$$

$$dF_z(r) = \left(\tfrac{1}{2}\rho\, c(r)\sqrt{V_{vent}^2 + r^2\omega^2}\right)\left(C_L(r)\omega r + C_D(r)V_{vent}\right)\, dr \qquad (6)$$

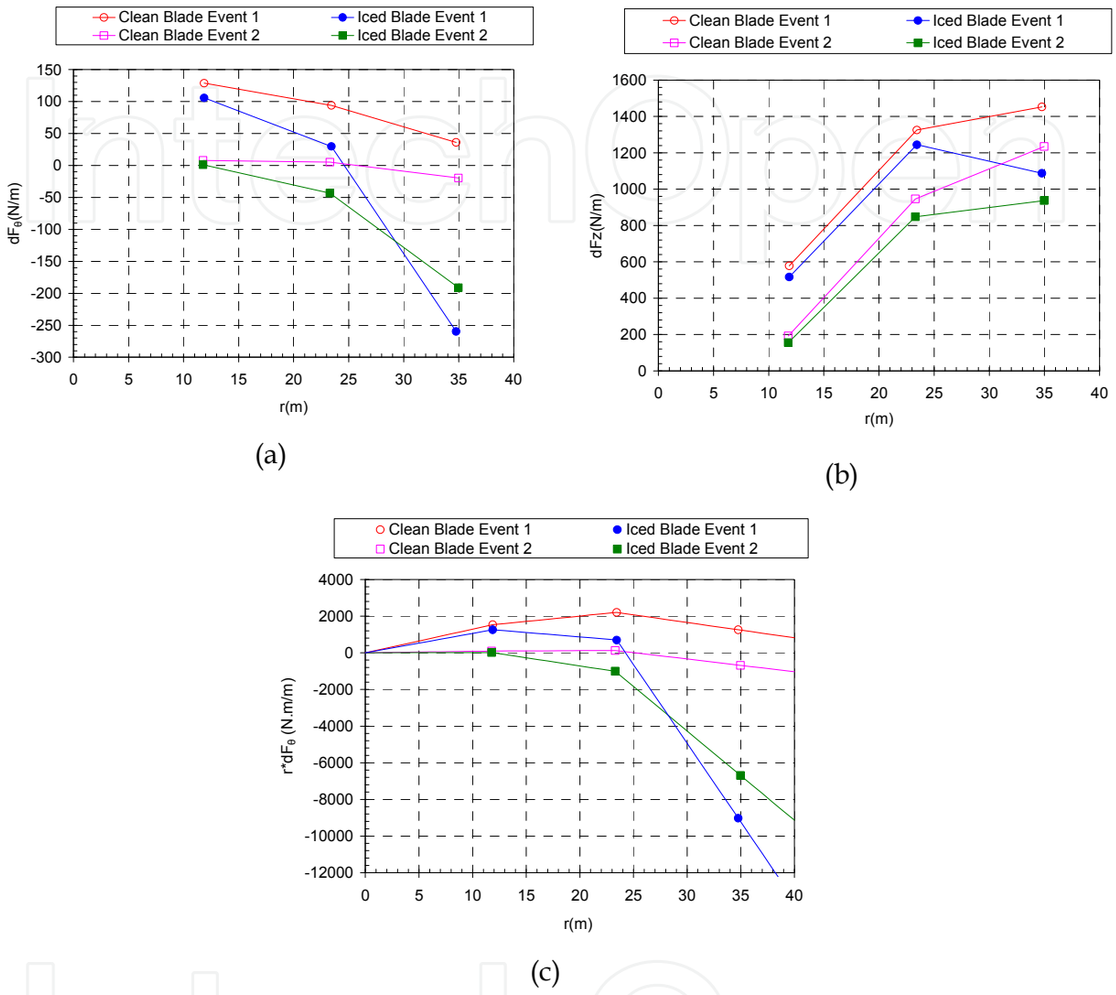

Fig. 10. (a) Distribution along the full size blade of the driving force per length unit dF_θ; (b) Distribution along the full size blade of the bending force per length unit dF_z and (c) Distribution along the full size blade of the torque per length unit r^*dF_θ

Here, *r is* the radial position in m, ρ the air density in kg/m³, *c* the blade chord in m, ωr the tangential speed in m/s, and V_{vent} the wind speed in m/s at the rotor disc entrance. The driving (dF_θ) and bending force (dF_Z) variation along the blade span are shown on Figure 10a and 10b. Figure 10c shows the torque distribution ($r \times dF_\theta$) linearly interpolated over the entire blade length in order to estimate the total torque. During both wet and dry accretion regimes, the driving and bending forces acting on the blade decrease, leading to a drastic torque reduction. In both cases, the drag force becomes so large compared to lift, that a negative torque occurs leading to rotor deceleration and possible stop. Torque reduction is more significant on the outer third of the blade so that the efficiency of a de-icing system would be increased in that region.

In Figure 11 we illustrate the variation of the total torque produced by the blade with the length of the de-icing system. The de-icing system is installed over a given length starting from the blade tip and the lift and drag coefficients of the clean airfoil are used where the de-icing system is operational. We notice again that the most efficient zone to be de-iced is near the blade tip as approximately 90% of the torque penalty compared to the clean blade is recuperated with only 30% length de-iced.

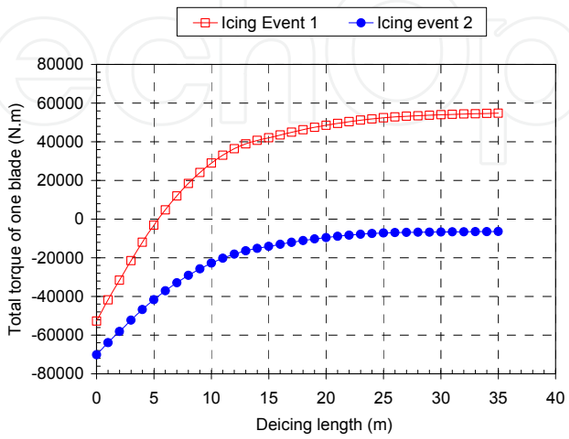

Fig. 11. Blade torque as a function of de-icing length, starting from the blade tip

5.4 Conclusion

The study provide the experimental assessment of the impact of glaze (icing event 1, wet regime) and rime (icing event 2, dry regime) on a wind-turbine blade. The liquid water content (LWC) for glaze accretion was 0.218 kg/m³, at -1.4 °C and 8.8 m/s wind speed, while the LWC for rime accretion was 0.242 kg/m³, at -5.7 °C and 4.2 m/s wind speed. In wet-regime (icing event 1), the angles of attack along the blade were 13° in average and glaze formed mostly at the leading edge and on the pressure side. Some ice accreted by runoff on the trailing edge for cinematic conditions corresponding to the blade airfoils located at the centre and the tip. In dry-regime (icing event 2), the angles of attack were below 9° and rime accreted mostly on the leading edge and partially on the pressure side for cinematic conditions of the blade airfoils located between the middle and the tip. The rime accreted on the leading edge was horn shaped, which considerably increased the surface roughness. The total mass of accumulated glaze on the blade was estimated to 709 kg (11% of the blade initial mass, which is 6500 kg) and the total mass of accumulated rime was estimated to 434 kg (6.7% of the blade initial mass). When glaze or rime accreted on the blade profile, lift decreased and drag increased. In both dry and wet regimes the lift reduction varied only slightly on the first two thirds of the blade, 9 %, but increased to 25 % on the last third, near the tip. The lift reduction at the blade tip was estimated at 40 % for both events. Drag increased along the blade following approximately a power law. The increase at the blade tip was in the order of 365 % for glaze and 250 % for rime. The amount by which lift decreased or drag increased depended on the quality, shape, and position of the ice. Finally, based on blade element model estimations, for both icing conditions the lift reduction and drag increase lead to a decrease in the bending and driving forces, and consequently a decrease in torque. The drag force becomes so important compared to lift

that the torque is negative, resulting in rotor deceleration and stop. Torque reduction is more significant on the outer third of the blade. Setting up a de-icing system on the last third of the blade only, would enable to decrease equipment and heating energy costs while maintaining 90% of the aerodynamic performance of the clean blade.

6. Experimental analysis and optimisation of an electro-thermal de-icing system

6.1 Scaling

Based on the results of the previous study on the effects of ice accretion on wind turbine performance, a second experimental study has been conducted to determine what would be the optimum positioning and functioning parameters for an electro-thermal de-icing system. The blade section is a NACA 63-415 airfoil, 0.5 m long with a 0.2 m chord. It is equipped with 12 resistant heating elements and instrumented with 12 thermocouples (Figure 2b). The meteorological parameters used for the experimental analysis of the de-icing system are presented In Table 7. These values have been scaled for simulation in the IWT (Figure 1). The main difference with the observed values is the colder temperature used in the IWT simulation which guarantees a rime ice along the blade. Rime ice is the most frequent during icing events in wind farms and it is the major cause of production losses.

LWC (g/m^3)	MVD (μm)	U_∞ (m/s)	T_{amb} (^oC)	T (min)
0.218	38.3	8	-10	360

Table 7. Characteristics of the icing event for the tests (full scale)

The blade geometry used for the testing corresponds to a Vestas V80 turbine of 1.8 MW. This type of wind turbine is presently installed where the meteorological data has been gathered. To simulate the icing event in the IWT, the icing conditions and the blade geometry need to be scaled. The wind speed selected for simulation is 8 m/s and corresponds to a configuration for which the angle of attack is 12° along most of the blade. The blade section is made of fibreglass and uses a NACA 63 415 airfoil. For the airfoil, 12° is the ideal angle of attack in terms of aerodynamic performance. All the tests were performed for this wind speed that corresponds to the maximal power coefficient of the wind turbine. Three different span positions on the real blade have been modelled. For the experimental value of the LWC in Table 1, the wind velocity in the IWT test section is limited to 40 m/s. Consequently the maximum span location that can be simulated is limited to 23 m. The relative velocity (V_{rel}) expressed in Equation (2) and simulated in the icing wind tunnel (IWT) is the combination of the wind velocity (V_{vent}) and the tangential velocity (V_{tang}) due to the rotation of the blade (Figure 3). The relation between the span position r and the relative velocity V_{rel} is obtained using the rotor disc theory (Burton et al. 2001). The wind speed that crosses the rotor plane (V_{vent}) is expressed in Equation (4) as a function of the free stream speed (V_∞) and the axial flow induction factor (a). The tangential velocity (V_{tang}) at the span location r is expressed in Equation (5) as a function of the rotational speed (ω), the span position r and the tangential flow induction factor (a'). Using the optimum value of the axial flow induction factors (a=1/3) the tangential flow induction factor becomes:

$$a' = \frac{U_\infty{}^2 a(1-a)}{\omega^2 r^2} \tag{8}$$

The relation between the span position and the relative wind speed simulated in the IWT is expressed as:

$$r = \frac{\omega\sqrt{U_{rel}{}^2 - U_w{}^2} + \sqrt{(U_{rel}{}^2 - U_w{}^2)\omega^2 - 4\omega^2 \bullet \frac{2}{9} U_\infty{}^2}}{2\omega^2} \quad (9)$$

Three different tests are performed considering a relative wind speed of 20m/s, 30m/s and 40m/s respectively. According to these calculations, Table 8 presents the corresponding span positions and the blade chord lengths for the selected IWT test section speeds. The chord length corresponds to the dimensions of the Vestas V80 wind turbine of 1.8 MW.

N° test	U_∞ (m/s)	U_{rel} (m/s)	r (m)	c (m)
1	8	20	10.6	2.7
2	8	30	16.6	2.3
3	8	40	22.5	1.8

Table 8. Corresponding real chord and span positions for the tests performed

According to the icing conditions and the geometry, the real characteristics are scaled using a scaling method developed by Anderson (Anderson, 2004). The Anderson scaling method gives excellent results for rime ice scaling. The experimental conditions for the three wind tunnel tests, corresponding to the span positions in Table 8, are presented in Table 9. The ice accretion in the wind tunnel is performed both with and without de-icing system working.

N° test	LWC (g/m^3)	MVD (μm)	α (°)	c (m)	U_{rel} (m/s)	T_{amb} (°C)	T (min)
1	0.4	26.7	12	0.2	20	-10	14.3
2	0.4	26.7	12	0.2	30	-10	16.9
3	0.4	26.7	12	0.2	40	-10	21.7

Table 9. Test conditions set for the IWT (each test number corresponds to the equivalent span position in Table 8)

6.2 Heating elements

The heating elements are Kapton flexible heaters with a wattage density of 10 W/po² (1.55 W/cm²). They are distributed on the airfoil as shown in Figure 12. The blade section is built in two parts in order to be able to open the airfoil if a technical problem with the thermocouples or the heating elements appears. The heating elements 0 and 3 are on the upper section and the heating elements 1 and 2 are on the lower section of the airfoil.

For each heating element, a thermocouple is placed between the surface and the heater (external thermocouple, referred as Th_e) and another one is placed inside and in front of the airfoil (internal thermocouple, referred as Th_i).

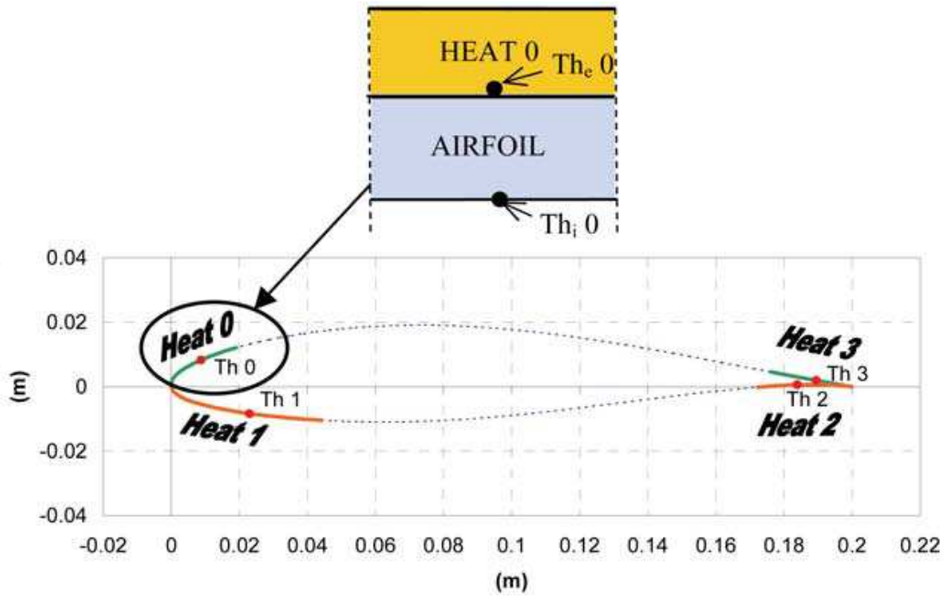

Fig. 12. Location of thermocouples and heating elements

6.3 Heating control

A computer controls the electric power sent to each heating element based on the temperature measured by the external thermocouples. The power consumed and the surface temperature of the system are recorded during the test. This allows studying the system's response depending on the icing condition applied. A comprehensive scheme of the de-icing system is presented in Figure 13.

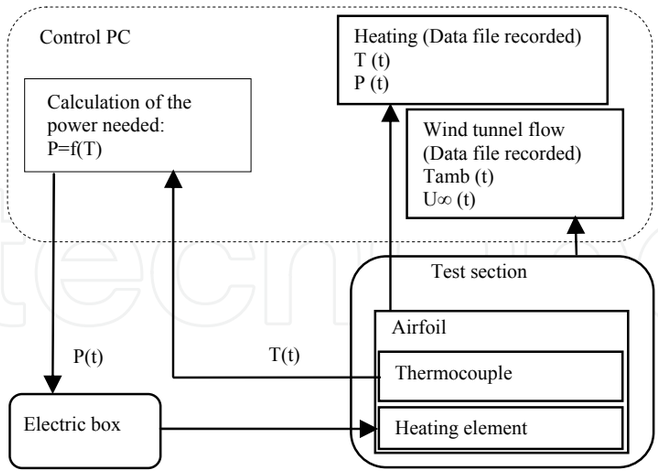

Fig. 13. Control Scheme of the De-Icing Control System

To optimize the power supplied to the heating elements, the amount of heat is related to the convective energy transfer during ice accretion at the blade surface. The other forms of energy transfer during ice accretion, which are adiabatic heating, conduction, evaporation and radiation, are all considered negligible compared to convection. The adiabatic heating is

low compared to the convection when the Mach number is less than 0.3. The conduction is negligible compared to the convection when the Biot number is high. Due to the low air temperature, little evaporation occurs during ice accretion and the radiation is negligible due to the clouds coverage during an icing event.
The power of the heating elements used on the airfoil's surface is expressed in Equation (10) and depends on the convective heat transfer coefficient h_1, the ambient, target and surface temperatures T_{amb}, T_c, T_h and the heating element area A:

$$P(t) = h_1 A(T_{amb} - T_c) + h_1 A(T_c - T_h) \tag{10}$$

The first right-hand-side term represents an approximation of the power needed for the de-icing and the second one represent the correction, considering the gap between the target and measured surface temperatures. The «heating coefficient» h_1 is approximated with the convective heat transfer coefficient, evaluated using a flat plate hypothesis given by Equation (11):

$$h_1 = \rho_{air}.c_{p_{air}}.U_{rel}.St \tag{11}$$

where the Stanton number is:

$$St = \frac{1}{2}.c_f \tag{12}$$

The friction coefficient is evaluated (Equation 13) for a turbulent flow because heating elements are located in the turbulent zone of the airfoil:

$$c_f = \frac{0.058}{\mathrm{Re}^{0.2}} \tag{13}$$

Finally the Reynolds number is:

$$\mathrm{Re} = \frac{\rho_{air}.U_{rel}.c}{\mu_{air}} \tag{13}$$

The target temperatures T_c for each test has been chosen so that we obtain a complete de-icing of all the heating elements surfaces during each test. The values of the different parameters used to calculate the power for each de-icing test are given in Table 10. With the increase of the wind speed (see each test parameters in Tables 8 and 9) the «heating coefficient» h_1 varies from 0.64 for Test 1 to 1.12 for Test 3. Also, the target temperature required for a complete de-icing of the heating elements 0 and 1 is different from the test 1 to 3.

N° test	h_1	T_c (°C) (Heat 0 and 1)	T_c (°C) (Heat 2 and 3)
1	0.64	5	1
2	0.88	10	1
3	1.12	15	1

Table 10. Test conditions set for the heating control

6.4 Results and analysis

De-Icing Results

The shapes and locations of the ice accretion on the surface are analysed in Figures 14 to 16 and illustrate the effectiveness of de-icing the wind turbine blade for the three test cases which parameters are indicated in Tables 8 to 10.

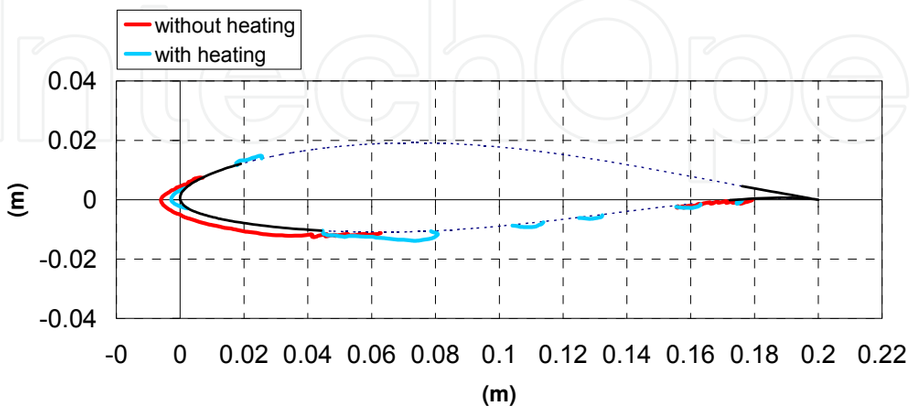

Fig. 14. Ice shape for Test 1 corresponding to r=10.6 m span position

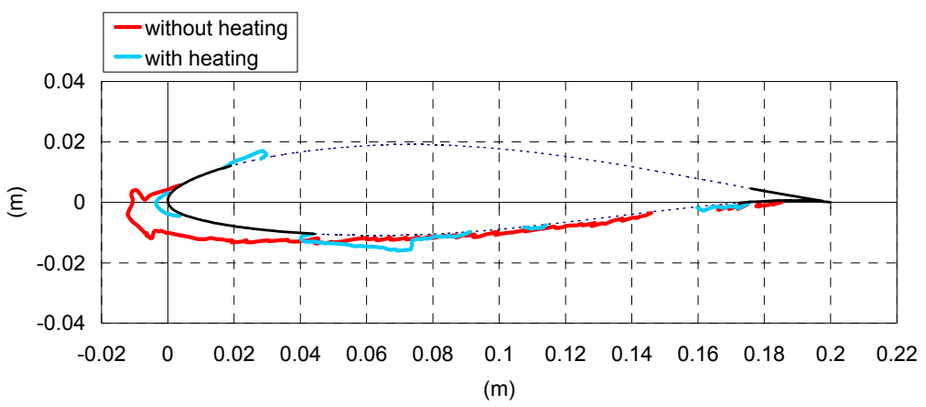

Fig. 15. Ice shape for Test 2 corresponding to r=16.6 m span position

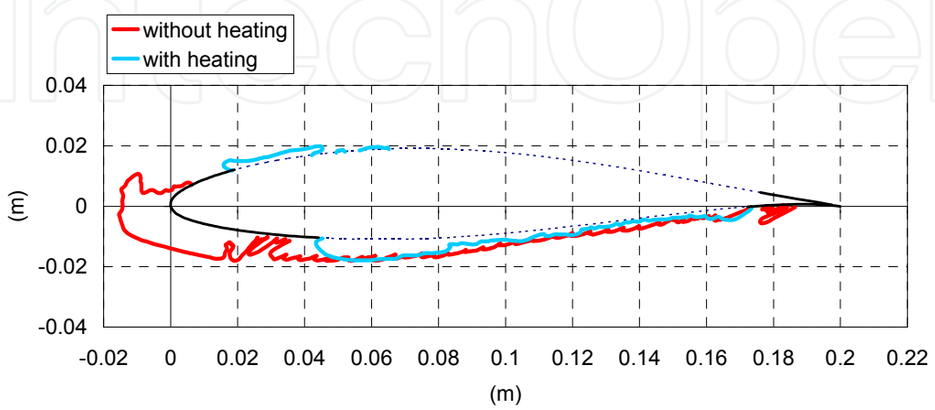

Fig. 16. Ice shape for Test 3 corresponding to r=22.5 m span position

Rime ice with milky appearance and characterized by a low density accretes on the airfoil during the tests without heating. This ice accretion is characteristic of a dry regime. On the other hand, the ice observed during the de-icing tests is transparent, with a high density, characteristic of glaze ice formed by runback water. Stream wise ice is observed at the leading edge for Test 1, corresponding to the span position nearest to the hub (10.6 m). For Tests 2 and 3, corresponding to a span position near the middle of the blade (16.6 m and 22.5 m), a protuberance with high roughness appears at the leading edge. Ice covers most of the lower surface of the airfoil at 16.6 m and covers completely the lower surface at 22.5 m.
For de-icing tests 1 and 2, corresponding to positions nearest to the hub (10.6m and 16.6 m) ice still accretes at the leading edge, probably because the heating elements number 0 and 1 are not exactly end-to-end. The liquid water at the leading edge runs back and refreezes at the end of the heating element to form a ridge. This is the worse inconvenient of the de-icing system. Leading edge is almost ice-free after de-icing. As the airfoil aerodynamic characteristics are more sensitive to the leading edge geometric modifications, aerodynamic performances should be better than for the iced airfoil without heating, but still worse than for a clean airfoil. This point needs more investigations to evaluate the real gain of the de icing.

Temperature Records

Figure 17 (a,b) illustrate temperature variation for icing tests without heating, while Figure 18 (a,b) illustrates results of the de-icing tests, with the de-icing system working. The temperatures measured by the thermocouples are recorded every 0.2 second during the whole test. These temperatures follow the icing wind tunnel (IWT) temperature variations as shown in Figure 17a. The IWT temperature variation is ±1 °C due to thermal inertia. The thermocouples have quick variations under short periods (26 s). This phenomenon is more significant for thermocouple 1 which is positioned in the zone of impacting droplets because of the high angle of attack of the blade. These quick temperature variations are partly due to the water spray ramp oscillations. The nozzles are fixed horizontally on the ramp, which moves up and down to insure a homogenous LWC in the test section. The ramp speed is about 0.08 m/s. When the ramp is in front of the airfoil, the surface collects more droplets and the temperature increases because of the liberation of latent heat of solidification. Thermocouple 0 is still warmer than thermocouples 2 and 3 for each icing test because of the smaller convection in this zone due to the high angle of attack. During the icing tests, the internal temperature is more stable than the external one, as shown in Figure 17b by thermocouples 1 and 3 in icing test 2. The temperature measured by thermocouple 1 decreases during the test. This is more obvious for tests 2 and 3 because of the important ice thickness collected at leading edge and due to ice insulation properties (Figures 15 and 17b).
For the de-icing tests, the surface temperature is strongly dependent on the heating. The recorded external temperatures follow the quick power variations (Figure 18a). The internal temperature measured by thermocouple 1 is less stable than that of the other thermocouples during the de-icing tests. This thermocouple is the most exposed to the impinging water droplets and the system has a short response time (Figure 18b). The external thermocouple 2 runs smoothly compared to the others (Fig. 11) while the internal thermocouple 2 temperature is more sensitive to the IWT temperature's variation than the other internal ones. This behavior is observed for all tests and is probably due to the small thickness of the airfoil in this area or to the contact between the thermocouple and a cold surface that increases the impact of the IWT.

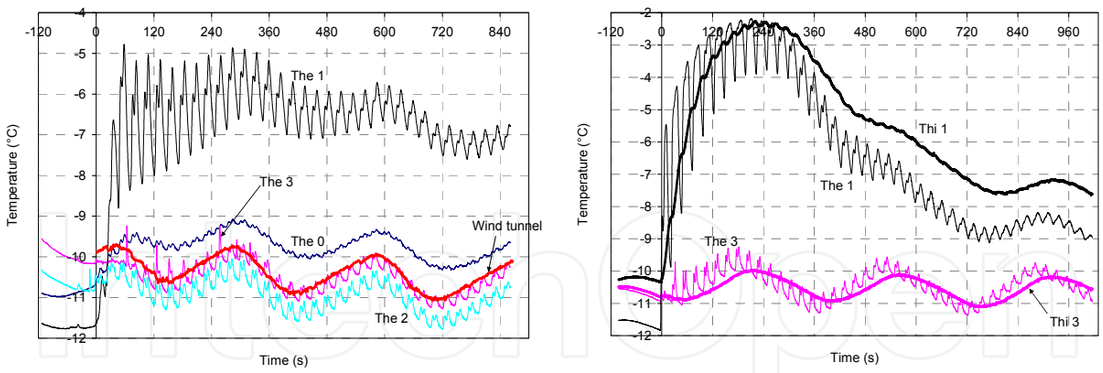

Fig. 17. (a): External and IWT temperature evolution for icing test 1 and (b): Temperature evolution of the internal and external thermocouples 1 and 3 for icing test 2

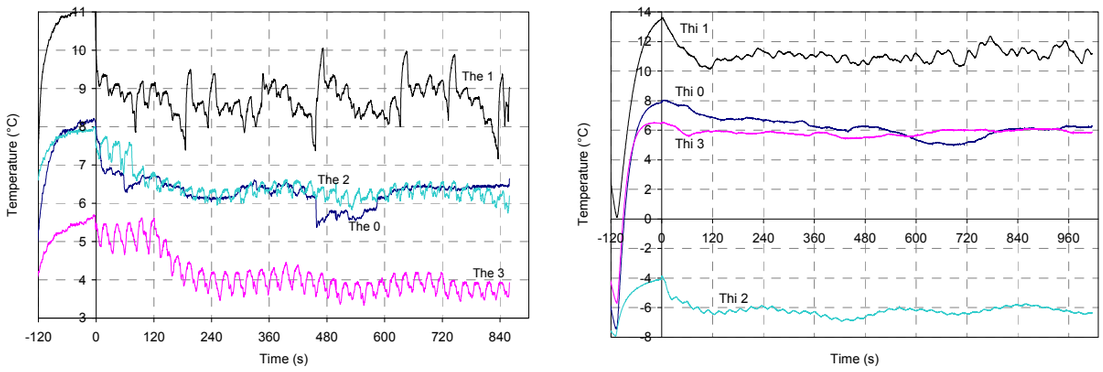

Fig. 18. (a): External temperature evolution for de-icing test 1 and (b): Internal temperature evolution for de-icing test 2

Power Consumption

The power is calculated and recorded every 0.2 second during the whole test. The power consumption varies from one test to another under the same experimental conditions because of the IWT temperature variations; these variations are lower than 2%. Due to the thermocouple's short response time, the quick power variations are instantaneously measured by the thermocouples and, as the temperature is then used for the heating control, this leads to rapid power variations. As an example, Figure 19a shows the variation of the power consumption for each element for de-icing test 1 which illustrates these fast variations. As for the temperature variation (Figure 18a), the power is less stable for heater 1 which is the most exposed to water droplets. Figure 19b shows the power consumed by every heating element for all tests parameters detailed in Tables 8 to 10 and corresponding to three different span positions. The power required for the de-icing increases with the radius of the span position. This is due to the increase of relative wind speed that has an important impact on the convective heat transfer of the airfoil. The system needs 3.5 to 3.9

more power near the tip position (22.5 m) than near the hub position (10.6 m) for the leading edge and 2.6 to 2.9 more power for the trailing edge. It needs 1.3 to 1.5 more power for the lower surface than for the upper surface. It is to be noted that heating element 3 is practically not useful for the test conditions selected in this study because of the high angle of attack and icing conditions. This heating element required more power than the heating element 2 due to the high convective heat exchange between the surface and the air.

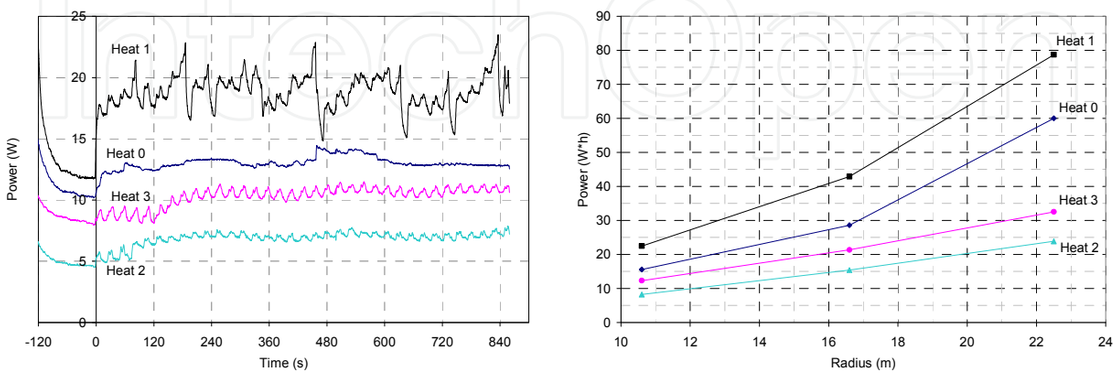

(a) (b)

Fig. 19. (a): Power consumption evolution of the heating elements during de-icing test 1 and (b): Heating elements power consumption at the 3 span positions

6.5 Conclusions

The design of the de-icing system is based on the different partial heating of four areas on the airfoil near the leading and the trailing edge and is subject to experimental limitations of IWT facilities. However the results are very encouraging. The de-icing is very efficient at keeping the leading edge free of ice, which is very important for the aerodynamic properties of the blade even if ridge ice forms at the end of the heating element. The airfoil instrumentation provided numerous results contributing to a better understanding of the process and further optimization of de-icing. As the time step of 0.2 s chosen for the power calculation lead to rapid variations of surface temperature, power calculation should be adjusted based on an average surface temperature computed over a longer period (1s or more). The results show that more energy is needed to de-ice the leading edge at the tip than at the hub (3.5 to 3.9 more), to de-ice the trailing edge at the tip than at the hub (2.6 to 2.9 more) and to de-ice the lower surface than the upper surface (1.3 to 1.5 more). It will be useful to confirm these wind tunnel results with full scale tests. The power control method leads to an optimization of the de-icing depending on the span position but the target temperatures need to be adjusted to obtain a clean airfoil.

7. Acknowledgments

This work represents a synthesis of over 5 years of collaboration between the Anti-icing Materials International Laboratory at the Université du Québec à Chicoutimi (Professors Jean Perron and Guy Fortin) and the Wind Energy Research Laboratory from the Université du Québec à Rimouski. Financial support from NSERC (Natural Sciences and Engineering

Research Council of Canada) and FQRNT (Fonds Québécois de Recherche sur la Nature et les Technologies) is kindly acknowledged. The author acknowledges also the contributions of graduate students, Olivier Parent, Clément Hochart and Christine Mayer.

8. References

Anderson, D.N. and Reich, A.D., 1997. Tests of the Performance of Coatings for Low Ice Adhesion. In: NASA (Editor), Aerospace Science Meeting and Exhibit, Reno, USA, pp. 14.

Anderson, D.N., 2004. *Manual of Scaling Methods*, NASA/CR-2004-212875, Ohio Aerospace Institute, Brook Park, Ohio, March 2004

Anonymous, 2004. *V80-1.8MW Pitch regulated wind turbine with OptiSlip and OptiTip*, General Specification, Technical document, Vestas, February 2004

Battisti, L., Baggio, P. and Fedrizzi, R., 2006. Warm-Air Intermittent De-Icing System for Wind Turbines. Wind Engineering, 30(5): 361-374.

Battisti, L., Brighenti, A., Dal Savio, S. and Dell'Anna, S., 2005a. Evaluation of Anti-Icing Energy and Power Requirement for Wind Turbine Rotors in Cold Climates, BOREAS VII. FMI, Saariselkä, Findland, pp. 13.

Battisti, L. and Fedrizzi, R., 2007. 2D Numerical Simulation of a Wind Turbine De-Icing System, Using Cycled Heating. Wind Engineering, 31(1): 33-42.

Battisti, L., Fedrizzi, R., Dell'Anna, S. and Rialti, M., 2005b. Ice Risk Assessment for Wind Turbine Rotors Equipped with De-Icing Systems, BOREAS VII. FMI, Saariselkä, Findland, pp. 11.

Boluk, Y., 1996. Adhesion of Freezing Precipitates to Aircraft Surfaces. Transport Canada, pp. 44.

Botta, G., Cavaliere, M. and Holttinen, H., 1998. Ice Accretion at Acqua Spruzza and its Effects on Wind Turbine Operation and Loss of Energy Production, BOREAS IV. FMI, Hetta, Finland, pp. 77-86.

Botura, G. and Fisher, K., 2003. Development of Ice Protection System for Wind Turbine Applications, BOREAS VI. FMI, Pyhätunturi, Finland, pp. 16.

Burton, T., Sharpe, S., Jenkins, N., Bossanyi, E., 2001. *Wind Energy Handbook,* John Wiley & Sons, LTD, 2001

Craig, D. and Craig, D., 1996. An Investigation of Icing Events on Haeckel Hill, BOREAS III. FMI, Saariselkä, Finland, pp. 169-193.

Dalili, N., Edrisy, A. and Carriveau, R., 2009. A Review of Surface Engineering Issues Critical to Wind Turbine Performance. Renewable and Sustainable Energy Reviews(13): 428-438.

Dobesch, H., Zach, S. and Tran, H.V., 2003. A New Map of Icing Potentials in Europe - Problems and Results, BOREAS VI. FMI, Pyhätunturi, Finland, pp. 9.

Fikke, S. et al., 2006. COST-727, Atmospheric Icing on Structures: 2006, Measurements and data collection on icing: State of the Art. MeteoSwiss, 75: 110.

Fikke, S.M., Säntti, K. and Laakso, T., 2005. Detectors for Atmospheric Icing, BOREAS VII. FMI, Saariselkä, Findland, pp. 8.

Fortin, G., Perron, J., Ilinca, A., 2005a. *A Study of Icing Events at Murdochville: Conclusions for the Wind Power Industry*, International Symposium "Wind Energy in Remote Regions", Magdalen's Island, October 2005

Fortin, G., Perron, J. and Ilinca, A., 2005b. Behaviour and Modeling of Cup Anemometers under Icing Conditions, IWAIS XI, Montréal, Canada, pp. 6.

Fortin, G., 2009. Thermodynamique de la Glace Atmosphérique. UQAC, pp. 9.

Gillenwater, D., 2008. Pertes de Puissance Associées aux Phénomènes Givrants sur une Éolienne Installée en Climat Nordique. Master Thesis, ÉTS, Montréal, Canada, 162 pp.

Harstveit, K., Tallhaug, L. and Fidje, A., 2005. Ice Accumulation Observed by Use of Web Camera and Modelled from Meteorological Parameters, BOREAS VII. FMI, Saariselkä, Findland, pp. 10.

Hochart, C., Fortin, G., Perron, J. and Ilinca, A., 2008. Wind Turbine Performance under Icing Conditions. Wind Energy(11): 319-333.

Homola, M.C., Nicklasson, P.J. and Sundsbo, P.A., 2006. Ice Sensors for Wind Turbines. Cold Regions Science and Technology(46): 125-131.

Horbaty, R., 2005. Wind Energy in Cold Climates - The Swiss Experience, BOREAS VII. FMI, Saariselkä, Findland, pp. 10.

ISO-12494, 2001. Atmospheric Icing of Structures. ISO copyrigth office, Geneva, Switzerland, pp. 56.

Jasinski, W.J., Noe, S.C., Selig, M.S. and Bragg, M.B., 1997. Wind Turbine Performance Under Icing Conditions, Aerospace Sciences Meeting & Exhibit. AIAA, Reno, USA, pp. 8.

Kimura, S., Sato, T. and Kosugi, K., 2003. The Effect of Anti-Icing Paint on the Adhension Force of Ice Accretion on a Wind Turbine Blade, BOREAS VI. FMI, Pyhätunturi, Finland, pp. 9.

Kimura, S., Tammelin, B. and Säntti, K., 2000. Estimation of Reduction of Power due to Icing from the Exixting Meteorological Data, BOREAS V. FMI, Levi, Finland, pp. 12.

Laakso, T. et al., 2003a. State-of-the-art of Wind Energy in Cold Climates. IEA Wind Annex XIX: 53.

Laakso, T., Peltola, E., Antikainen, P. and Peuranen, S., 2003b. Comparison of Ice Sensors for Wind Turbines, BOREAS VI. FMI, Pyhätunturi, Finland, pp. 11.

Laakso, T. and Peltola, E., 2005a. Review on Blade Heating Technology and Future Prospects, BOREAS VII. FMI, Saariselkä, Finland, pp. 12.

Laakso, T. et al., 2005b. Wind Energy Projects in Cold Climates. International Energy Agency: 36.

Maissan, J.F., 2001. Wind Power Development in Sub-Arctic Conditions with Severe Rime Icing, Circumpolar Climate Change Summit and Exposition, Whitehorse, Canada, pp. 18.

Makkonen, L. and Ahti, K., 1995. Climatic Mapping of Ice Loads Based on Airport Weather Observations. Atmospheric Research, 36: 185-193.

Makkonen, L. and Autti, M., 1991. The Effects of Icing on Wind Turbines, EWEC, Amsterdam, Netherlands, pp. 575-580.

Makkonen, L., Laakso, T., Marjaniemi, M. and Finstad, K.J., 2001. Modelling and Prevention of Ice Accretion on Wind Turbines. Wind Engineering, 25(1): 3-21.

Mansson, J., 2004. Why De-Icing of Wind Turbine Blades?, Global Windpower, Chicago, USA, pp. 12.

Marjaniemi, M. et al., 2000. Wind Turbines in Light Icing Conditions - Experience of the Pori 8 MW Wind Farm, BOREAS V. FMI, Levi, Finland, pp. 13.

Marjaniemi, M. and Peltola, E., 1998. Blade Heating Element Design and Practical Experiences, BOREAS IV. FMI, Hetta, Finland, pp. 197-209.

Mayer, C., 2007. Système Électrothermique de Dégivrage pour une Pale d'Éolienne. Master Thesis, UQAR, Rimouski, Canada, 193 pp

Mayer, C., Ilinca, A., Fortin, G. and Perron, J., 2007. Wind Tunnel Study of Electro-Thermal De-Icing of Wind Turbine Blades. International Journal of Offshore and Polar Engineering, 17(3): 182-188.

McKittrick, L R, Cairns, D S, Mandell, J, Combs, D C, Rabern, D A, Van Luchene, R D (2001). *Analysis of a Composite Blade Design for the AOC 15/50 Wind Turbine Using a Finite Element Model*, Sandia National Laboratories.

Patreau, V., Morency, F. and Paraschivoiu, I., 1998. Analysis of Thermal De-Icing System for Horizontal Axis Wind Turbine Blade, BOREAS IV. FMI, Hetta, Finland, pp. 222-235.

Peltola, E., Laakso, T., Antikainen, P. and Peuranen, S., 2003. Prevention of Icing Effects, BOREAS VI. FMI, Pyhätunturi, Finland, pp. 9.

Peltola, E., Marjaniemi, M., Kaas, J. and Aarnio, E., 1996. Pyhätunturi Operational Experiences, BOREAS III. FMI, Saariselkä, Finland, pp. 131-144.

Pinard, J.-P. and Maissan, J.F., 2003. Experience from Use of Heated Wind Sensors and Rime Ice Detectors over the Past 12 Years, BOREAS VI. FMI, Pyhätunturi, Finland, pp. 7.

Richert, F., 1996. Is Rotorcraft Icing Knowledge Transferable to Wind Turbines?, BOREAS III. FMI, Saariselkä, Finland, pp. 366-380.

Seifert, H., Richert, F., 1997. *Aerodynamics of iced airfoils and their influence on loads and power production*, Germany, 1997.

Seifert, H., 2003. Technical Requirements for Rotor Blades Operating in Cold Climate, BOREAS VI. FMI, Pyhätunturi, Finland, pp. 13.

Stallabrass, J.R., 1978. *An Appraisal of the single Rotating Cylinder Method of Liquid Water Content Measurement*, Canadian Research Council Report, LTR-L T-92, November 1978.

Tallhaug, L., 2003. Calculation of Potential Ice Risk in Norway, BOREAS VI. FMI, Pyhätunturi, Finland, pp. 8.

Tammelin, B. et al., 2000. Wind Energy Production in Cold Climate (WECO). 41, FMI, Helsinki, Finland.

Tammelin, B. and Säntti, K., 1994. Effect of Rime Accretion on Wind Energy Production in the Top Areas of Fells, BOREAS II. FMI, Pyhätunturi,Finland, pp. 265-275.

Tammelin, B. and Säntti, K., 1996. Estimation of Rime Accretion at High Altitudes - Preliminary Results, BOREAS III. FMI, Saariselkä, Finland, pp. 194-210.

Tammelin, B. and Säntti, K., 1998. Icing in Europe, BOREAS IV. FMI, Hetta, Finland, pp. 125-132.

Tammelin, B. et al., 2005. Wind Turbines in Icing Environment: Improvement of Tools for Siting, Certification and Operation - NEW ICETOOLS. FMI: 127.

Weis, T.M. and Maissan, J., 2003. The Effects of Black Blades on Surface Temperatures for Wind Turbines, Pembina Institute.

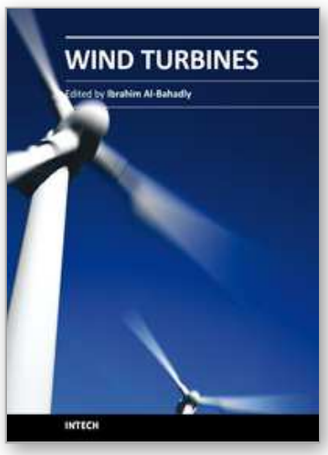

Wind Turbines

Edited by Dr. Ibrahim Al-Bahadly

ISBN 978-953-307-221-0
Hard cover, 652 pages
Publisher InTech
Published online 04, April, 2011
Published in print edition April, 2011

The area of wind energy is a rapidly evolving field and an intensive research and development has taken place in the last few years. Therefore, this book aims to provide an up-to-date comprehensive overview of the current status in the field to the research community. The research works presented in this book are divided into three main groups. The first group deals with the different types and design of the wind mills aiming for efficient, reliable and cost effective solutions. The second group deals with works tackling the use of different types of generators for wind energy. The third group is focusing on improvement in the area of control. Each chapter of the book offers detailed information on the related area of its research with the main objectives of the works carried out as well as providing a comprehensive list of references which should provide a rich platform of research to the field.

InTech Europe
University Campus STeP Ri
Slavka Krautzeka 83/A
51000 Rijeka, Croatia
Phone: +385 (51) 770 447
Fax: +385 (51) 686 166
www.intechopen.com

InTech China
Unit 405, Office Block, Hotel Equatorial Shanghai
No.65, Yan An Road (West), Shanghai, 200040, China
中国上海市延安西路65号上海国际贵都大饭店办公楼405单元
Phone: +86-21-62489820
Fax: +86-21-62489821

IntechOpen